MODELING OF ACID FRACTURING IN CARBONATE RESERVOIRS

A Thesis

by

MURTADA SALEH H AL JAWAD

Submitted to the Office of Graduate and Professional Studies of
Texas A&M University
in partial fulfillment of the requirements for the degree of

MASTER OF SCIENCE

Chair of Committee,	Ding Zhu
Committee Members,	Alfred Daniel Hill
	Marcelo Sanchez
Head of Department,	Alfred Daniel Hill

August 2014

Major Subject: Petroleum Engineering

ABSTRACT

The acid fracturing process is a thermal, hydraulic, mechanical, and geochemical (THMG)-coupled phenomena in which the behavior of these variables are interrelated. To model the flow behavior of an acid into a fracture, mass and momentum balance equations are used to draw 3D velocity and pressure profiles. Part of the fluid diffuses or leaks off into the fracture walls and dissolves part of the fracture face according to the chemical reaction below.

$$2H^+(aq) + CO_3^{2-} \rightarrow H_2CO_3(aq) \rightarrow CO_2(g) + H_2O\ (l)$$
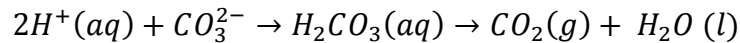
An acid balance equation is used to draw the concentration profile of the acid and to account for the quantity of rock dissolved. An algorithm is developed for this process to generate the final conductivity distribution after fracture closure. The objective of modeling acid fracturing is to determine the optimum condition that results in a petroleum production rate increase.

The conductivity value and acid penetration distance both affect the final production rate from a fracture. Treatment parameters are simulated to draw a conclusion about the effect of each on the conductivity and acid penetration distance. The conductivity distribution file from an acid fracturing simulator is imported into the ECLIPSE reservoir simulator to estimate the production rate. Reservoir permeability is the determining factor when choosing between a high- conductivity value and a long penetration distance.

For the model to be more accurate, it needs to be coupled with heat transfer and geomechanical models. Many simulation cases cannot be completed because of numerical errors resulting from the hydraulic model (Navier-Stokes equations). The greatest challenge for the simulator before coupling it with any other phenomena is building a more stable hydraulic solution.

DEDICATION

To my family

ACKNOWLEDGEMENTS

NOMENCLATURE

A	Fracture face area
$\tilde{C}$	Average acid concentration
C_1, C_2	Constants in equation 1.1
C_A, C	Acid concentration
C_c	Reservoir fluid viscosity / compressibility coefficient
C_{eqm}	Equilibrium concentration
C_{fD}	Dimensionless fracture conductivity
C_{HCl}	Hydrochloric acid concentration
C_t	Overall leakoff coefficient
c_t	Total compressibility
C_v	Effluent viscosity and relative permeability coefficient
C_{vc}	$C_v + C_c$
$C_{v,wh}$	Effluent viscosity coefficient with wormhole
C_w	Wall building coefficient
D_{eff}, D_A	Acid diffusion coefficient
$DREC$	Dissolved rock equivalent conductivity, md-ft
E	Young Modulus
E_f	Reaction rate constant
E_f°	Reaction rate constant at reference temperature

f	Fraction of acid leakoff to react with fracture surface
$f_{calcite}$	Percentage of calcite in the formation
F_{cv}	Ratio of filter cake to filtrate volume
H	Fracture height
J	Productivity index
J_y^A	Acid diffusion flux in width direction
K	Consistency index
k	Reservoir permeability
k_i	Relative permeability of formation to effluent fluid
k_r	Formation permeability relative to mobile reservoir fluid
L	Acid penetration distance
MW	Molecular weight
n	Power law index
N_{pe}	Peclet number
P	Pressure inside fracture
P_{in}	Fracture inlet pressure
P_{out}	Fracture outlet pressure
Q_{ibt}	Number of pore volume injected at wormhole breakthrough time
q, q_{in}, i	Injection rate
R	Universal gas constant
RES	Rock embedment strength
s	Closure stress

T	Reservoir temperature
t	Time
u_A°	Average x-direction velocity inside the fracture
$\tilde{u}_N$	Average leakoff velocity
v	Stoichiometric coefficient
v_L, u_N	Leakoff velocity
v_x	x-direction velocity component
v_y	y-direction velocity component
v_z	z-direction velocity component
$\tilde{w}$	Average fracture width
w_i	Ideal fracture width
wk_f	Fracture conductivity, md-ft
$(wk_f)_0$	Fracture conductivity at zero closure stress
x	Direction parallel to fracture length
x_f	Fracture half length
y	Direction parallel to fracture width
y_1, y_2	Position on fracture face
z	Direction parallel to fracture height
α	Order of reaction
β	Gravimetric dissolving power
ΔE	Activation energy

$\tilde{\eta}$	Dimensionless width number
λ_D	Normalized correlation length
λ_n, G_n	Eigenvalues
σ_D	Normalized standard deviation
φ	Formation porosity
ρ	Density
μ	Fluid viscosity
μ_a	Viscosity of effluent fluid
μ_f	Viscosity of mobile formation fluid
μ_{app}	Apparent viscosity for power law fluid
$\mathcal{X}$	Dissolving power

TABLE OF CONTENTS

LIST OF FIGURES

LIST OF TABLES

CHAPTER I

INTRODUCTION

1.1 Introduction

Acid fracturing is a well stimulation method used in carbonate formations to enhance the oil production rate. Acid fracturing consists primarily of three stages: preflush, pad-acid injection, and overflush. In the preflush stage, viscous slick water is used to initiate the fracture and to reduce the temperature of the fracture walls. The pad and acid are injected in stages to propagate the fracture and to etch the fracture walls. Overflush is used to move the acid deeper into the fracture to improve the acid penetration distance. Because of formation stresses, the fracture closes and the job success depends on the amount of conductivity created after closure and the length of the etched fracture.

Acid tends to etch the fracture wall in a nonuniform pattern because of the rock heterogeneity. This phenomenon prevents complete fracture closure because of the wall roughness and the asperities hold the fracture open. It is difficult to predict accurately the fracture conductivity value because fracture heterogeneity cannot be captured from field data. Laboratory experiments are conducted to measure the fracture conductivity in small core samples; however, this fracture conductivity scarcely represents the entrance of a fracture. Conductivity correlations developed from either laboratory data or theoretical studies usually show large errors when compared with field results or other

experimental data. In such stochastic processes, it is not unusual to find discrepancies in terms of stimulation ratio between field results and acid design calculations.

The design of an acid fracturing treatment is accomplished by estimating the optimum conductivity and acid penetration distance that results in maximum benefit of the treatment. Design parameters include selecting the fluid types, number of stages, pumping rate, and injection time. Changing these parameters results in different fracture geometry, etching patterns, and acid-penetration distance. A complete study of formation fluid properties, mineralogy and permeability distributions, and formation temperature should be conducted prior to the stimulation operation. Simulators are usually used to estimate how these design parameters affect the stimulation job.

1.2 Literature Review

Using acid to stimulate a carbonate formation is not a recent practice. In 1895, Standard Oil Company used concentrated hydrochloric acid as a stimulation fluid to enhance oil production from the Lima formation in Ohio. The first observation of the effects of acid fracturing occurred in 1935. At that time, Schlumberger stimulated a reservoir by acid injection where the formation was determined to be fractured when the pressure reached "lifting pressure". Acid fracturing became an accepted stimulation method for carbonate reservoirs to improve production not achievable by matrix treatment alone (Kalfayan, 2007).

Propped fracturing is another stimulation method used in carbonate formations. In many cases, propped fracturing is preferred over acid fracturing because conductivity

is preserved longer. Designing propped fracturing is more convenient and predictable than acid fracturing because reactive fluids are not used in the process, which makes it easy to predict the formation conductivity. Many researchers have provided an application window for each technique but there are no strict guidelines. Acid fracturing is usually preferred when the formation is shallow and very heterogeneous to maintain conductivity after fracture closure. One advantage of acid fracturing is the low probability of job failure because early screenout is not possible in this case.

One of the first acid-fracturing conductivity calculations was performed by Nierode and Kruk (1973). They stated that conductivity is difficult to predict because of rock heterogeneity due to the fact that laboratory experiments represent only the entrance of the fracture. In correlating the calculations and laboratory experimental results, Nierode and Kruk concluded that conductivity is function of the amount of dissolved rock (DREC), rock embedment strength (RES), and formation closure stress (s). The correlation was based on 25 laboratory experiments with small cores that were cut under tension to produce rough surfaces. The Nierode and Kruk conductivity correlation is shown in Eqs. 1.1-1.3:

$$wk_f = C_1 \exp(-C_2 s) \dots\dots\dots\dots\dots\dots\dots\dots\dots\dots\dots\dots\dots\dots\dots\dots \text{(1.1)}$$

$$C_1 = 0.265 \, (DREC)^{0.822} \dots\dots\dots\dots\dots\dots\dots\dots\dots\dots\dots\dots\dots\dots\dots \text{(1.2)}$$

$$C_2 * 10^3 = \begin{cases} 19.9 - 1.3\ln(RES) & 0 < RES < 20{,}000 psi \\ 3.8 - 0.28\ln(RES) & 20000 \leq RES \leq 500{,}000 \, psi \end{cases} \dots\dots\dots\dots \text{(1.3)}$$

This correlation represents the lower bound of conductivity when compared with field values as suggested by Nierode and Kruk. Numerous commercial software

programs use this correlation where parameters can be easily obtained from field data or core analysis. Since 1973, several correlations were developed based on theoretical or empirical background (Gangi, 1978; Walsh, 1981; Gong et al., 1999; Pounik, 2008). Even though the Nierode and Kruk work is the standard in the oil industry, it fails to capture the significant impact of formation heterogeneity on fracture conductivity. Deng et al. (2012) attempted to include the effect of formation heterogeneity in their theoretical correlation. They stated that permeability and mineralogy distribution are the reasons for differential etching in carbonate rocks. Three parameters are used to characterize permeability distribution: the correlation lengths in horizontal ($\boldsymbol{\lambda}_{D,x}$) and vertical ($\boldsymbol{\lambda}_{D,z}$) directions and the normalized standard deviation of permeability (σ_D). The correlation length in the x direction has higher value because of the natural bedding in that direction. The higher the $\boldsymbol{\lambda}_{D,x}$, the higher the conductivity because of the fracture channels that are difficult to close. A high $\boldsymbol{\lambda}_{D,z}$ results in low conductivity because fracture-isolated openings contribute less to the flow in the fracture. A high σ_D means better width distribution, resulting in harder to close channels, which means better fracture conductivity. Mineralogy distribution depends on the percentage of calcite and dolomite in the rock. The higher the percentages of calcite, the more opening are the channels when the fracture closes, which means higher conductivity. The optimum percentage for calcite is 50%; however, conductivity decreases for higher calcite percentages. Rock mechanical properties have an impact on conductivity, especially Young's modulus, where higher values result in higher conductivity. Variation in Poisson's ratio does not have a significant impact on conductivity; therefore, a typical

value of 0.3 is used. The correlations developed are divided into three cases: permeability distribution, mineralogy distribution, and a competing case between the two.

To estimate the well productivity improvement, two parameters should be provided: 1) the ratio of fracture length to drainage radius; and 2) the ratio of fracture conductivity to the formation permeability (McGuir and Sikora, 1960). Acid penetration distance in reactive formations ranges from a maximum penetration distance case where the pad fluid is assumed to control the leakoff rate (reaction rate limit) and a minimum penetration distance where acid viscosity is assumed to control acid leakoff (fluid loss limit). Because the reaction rate between hydrochloric acid (HCl) and a carbonate formation occurs so quickly, the process of rock etching is controlled by the acid mass transfer to the fracture wall, which is the slower step. Fluid loss additives and acid retarders are usually added to an acid system to enhance etching performance and acid penetration distance.

Designing an acid-fracturing job nowadays is performed by using simulators. Before simulators, analytical solutions of velocity and concentration profiles in 1D or 2D were used and a simple procedure was implemented. Nierode and Williams (1972) suggested a design procedure to predict stimulation ratio. The procedure began by calculating acid penetration distance from a chart (Fig.1.1) using Peclet number and a specific acid concentration value to read the dimensionless acid penetration number. The Peclet number, N_{Pe}, is given in the equation below:

$$N_{Pe} = \frac{\tilde{u}_N \tilde{w}}{2D_A} \dots\dots\dots\dots\dots\dots\dots\dots\dots\dots\dots\dots\dots\dots\dots\dots\dots\dots\dots\dots\dots\dots\dots \text{(1.4)}$$

where $\tilde{u}_N$ is the average leakoff velocity, $\tilde{w}$ is the fracture average width, and D_A is the effective mixing acid diffusion coefficient. The effective mixing diffusion coefficient (larger than the ion diffusion coefficient) is calculated using a correlation that is a function of the Reynold's number and fracture width. An example is presented in the Nierode and Williams (1972) paper to show how the calculation predicts a production improvement. Average values for velocity and concentration are used in these calculations, and the charts presented are limited to few cases that only imitate the laboratory condition. This method is based on up-scaling laboratory results from small sized cores to represent hundreds of feet of fracture.
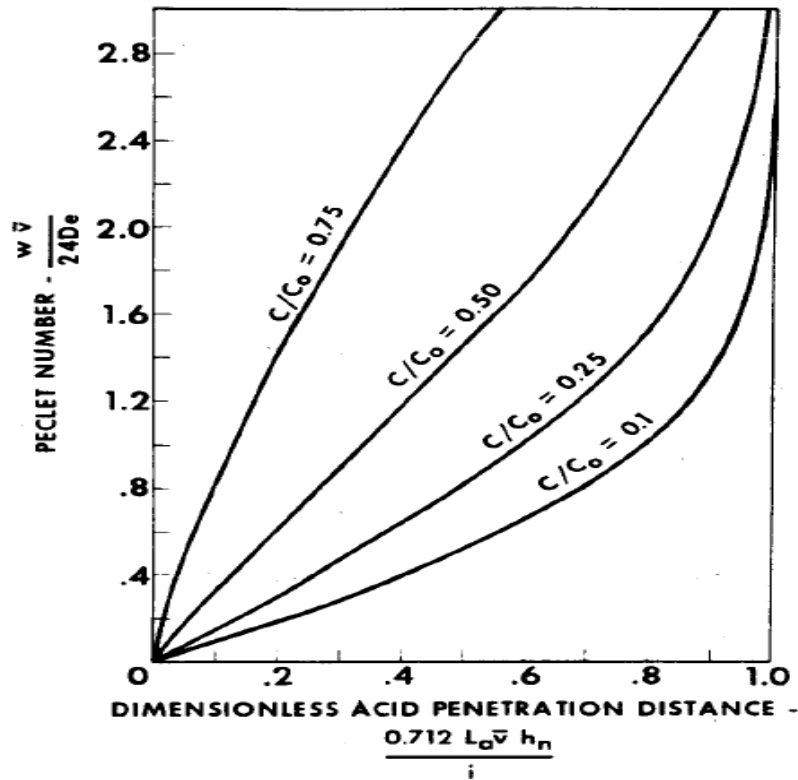
Figure 1.1: Acid penetration distance as function of Peclet number and acid concentration (Williams and Nierode, 1972).

Schechter provided a theoretical approach to design an acid-fracturing job (Schechter, 1992). The Berman solution was used by Schechter for the velocity profiles in the x, y directions satisfied both the continuity and the Navier-Stokes equations. These 2D analytical solutions are presented in Eqs. 1.5-1.7:

$$u(x, y) = [u_A^0 - < u_N^- > x]f'(\tilde{\eta}) \dotfill (1.5)$$

$$v(x, y) = < u_N^- > f(\tilde{\eta}) \dotfill (1.6)$$

$$u_A^0 = \frac{i}{2\widetilde{w}H} \text{ and } \tilde{\eta} = \frac{2y}{\widetilde{w}} \dots\dots\dots\dots\dots\dots\dots\dots\dots\dots\dots\dots\dots\dots\dots \text{ (1.7)}$$

where u, v are velocities in the x, y directions, u_A^0 is the average velocity inside the

fracture, i is the acid injection rate, H is the fracture height, and $\tilde{\eta}$ is a dimensionless

number for acid position in a fracture width direction. The acid mass balance equation is

used to calculate concentration as function of the x- direction where the y-direction

concentration values are averaged. The acid mass balance equation and the analytical

solutions are shown in Eqs.1.7-1.8:

$$u(x,y)\frac{\partial c}{\partial x} + v(x,y)\frac{\partial c}{\partial y} = D_A \frac{\partial^2 c}{\partial y^2} \dots\dots\dots\dots\dots\dots\dots\dots\dots\dots\dots\dots \text{ (1.8)}$$

$$\frac{\check{C}}{C_i} = \sum_{n=0}^{\infty} G_n (1 - \frac{x}{L})^{2\lambda_n^2/3NPe} \dots\dots\dots\dots\dots\dots\dots\dots\dots\dots\dots \text{ (1.9)}$$

where λ_n and G_n are eigenvalues, C is the acid concentration, $\check{C}$ is the average acid

concentration, C_i is the initial acid concentration, and L is the acid penetration distance.

From the solution presented in Figure 1.2 for a Peclet number greater than one, the case

is the fluid loss limit where the fluid completely leaks off before the acid is exhausted.

When the Peclet number is less than one, it is reaction-limit controlled and the acid is

consumed before the fluid leaks off. This analytical solution has a limitation in terms of

Peclet values and Reynolds numbers. In general, the solution assumptions are: laminar

flow and infinite reaction rate while wall roughness and secondary flow effects are

neglected. The length (L) in this case may not be the actual fracture half-length but is the

acid-penetration length that will satisfy the volume balance equation (injection rate =

fluid loss rate). The ideal fracture width is calculated as a function of fracture length (x)

8

where the Terrill (1964) acid solution is used for width calculations. It is found that the

higher the Peclet number, the more distributed is the etching along the fracture. Width

distribution as a function of distance is shown in Eq. 1.10:

$$w_i = -\frac{\beta i t_A C_i}{2\rho_f H(1-\varphi)} \frac{d}{dx}\left[(1-\frac{x}{L})\frac{\tilde{C}}{C_i}\right]\dots\dots\dots\dots\dots\dots\dots\dots\dots\dots\dots\dots\dots\dots\dots (1.10)$$

where w_i is the ideal fracture width, ρ_f is the fluid density, φ is the formation porosity,

t_A is the total time of acid injection, and β is the gravimetric dissolving power. An

equation for an optimum penetration distance is suggested assuming the fracture is

equally etched along its length. The equation used is an analogue to that of the prop

fracture case. Selecting acid viscosity can determine the acid leakoff coefficient; hence,

the acid injection rate and the penetration distance. An issue with acid fracturing design

is the Peclet number that gives optimum penetration distance may not give optimum

uniform etching.
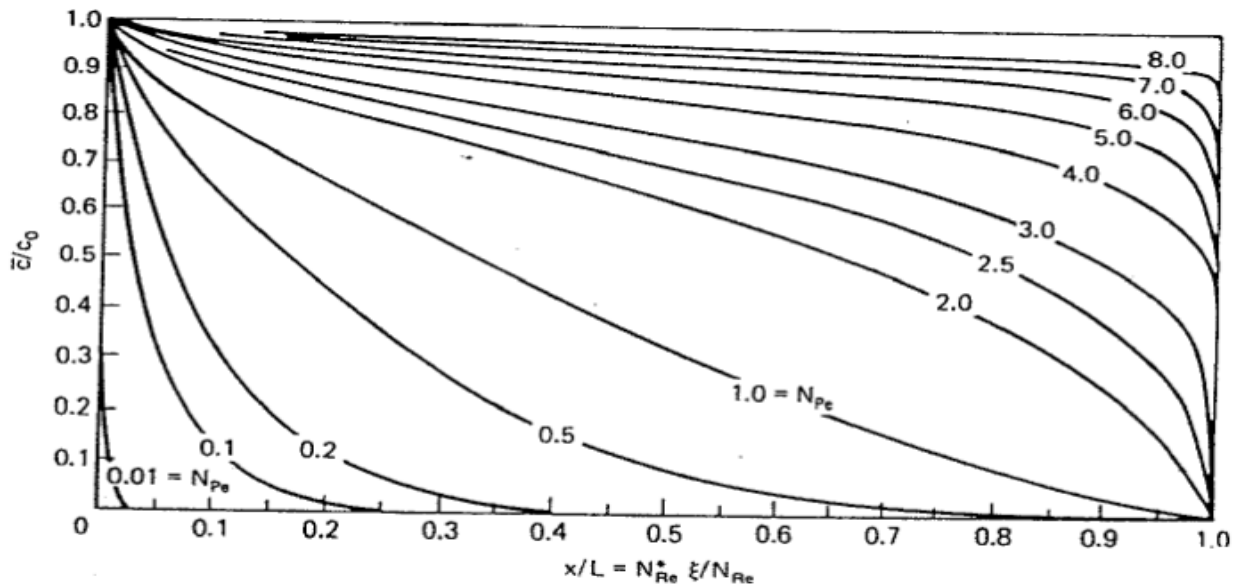
Figure 1.2: Acid penetration distance as function of concentration and Peclet number (Schecter, 1992).

Modeling acid fracturing is a necessity to provide more accurate results of acid convection, diffusion, and reaction with the fracture walls. Determining fracture geometry is a first step where many different models can be used in this aspect. Dean and Lo (1989) calculated the fracture length by assuming Perkins-Kern-Nordgren (PKN) fracture shape. An acid transport model is introduced by Dean and Lo (1989) where the 2D continuity equation and acid mass balance equation are implemented and reaction rate is assumed to be infinite. Settari (1993) developed a more comprehensive model that accounted for different fluids with different rheologies, mass transfer and rate of reaction limited cases, wormholing effect in leakoff calculations, heat of reaction, and coupling of fracture geometry. Gdanski and Lee (1989) provided a model that took care of the gross assumptions in fracture acidizing, such as infinite reaction rate, no heat of

10

reaction, constant average fracture temperature, no convection effect, and single stage geometry.

The number of pore volumes (PV) to breakthrough is very important in determining the effect of wormholing. Normally, carbonate formations have small PVs while dolomite has higher PVs to breakthrough; hence, the effect of wormholing is significant in carbonate reservoirs, especially in gas fields. Leakoff parameters are important in the solution of acid penetration distance and acid fracturing conductivity. A volumetric method introduced by Economides et al. (1994) is used where flow is linear and wormholes are short. For short wormholes, the wormhole growth is almost linear with fluid flux. Parameters are varied in experimental work to account for wormholing, including acid concentration, injection rates, and temperature. Pressure drop is measured against PV and found to be almost linear, which means that wormhole growth is almost linear in the case of carbonates. In dolomite, the growth is not linear and the PV value can be as high as 50. Experiments showed that there is an optimum value for injection rate where PV is at minimum. It is safe to increase the injection rate because the increase in PV is gradual and small. Assuming a constant injection rate and constant growth velocity of wormholes, the length of the wormhole is correlated with the injection rate. Formation zones are divided into filter cake, Cw, wormhole and invaded zone, Cv, and compressed reservoir zone, Cc, as shown in Figure 1.3. Wormholes will affect only the fluid loss in the invaded zones and pressure drop is assumed to be negligible in wormholes when compared with the matrix. For those reasons, the only change that accounts for including wormholing is in the viscous fluid loss coefficient

11

Cv. When the number of pore volumes injected is equal to 1, the fluid front in the invaded zone is equal to the length of the wormholes. Then, a method was introduced to calculate the effect of wormholing in the overall fluid loss coefficient (Zhu and Hill, 1995)
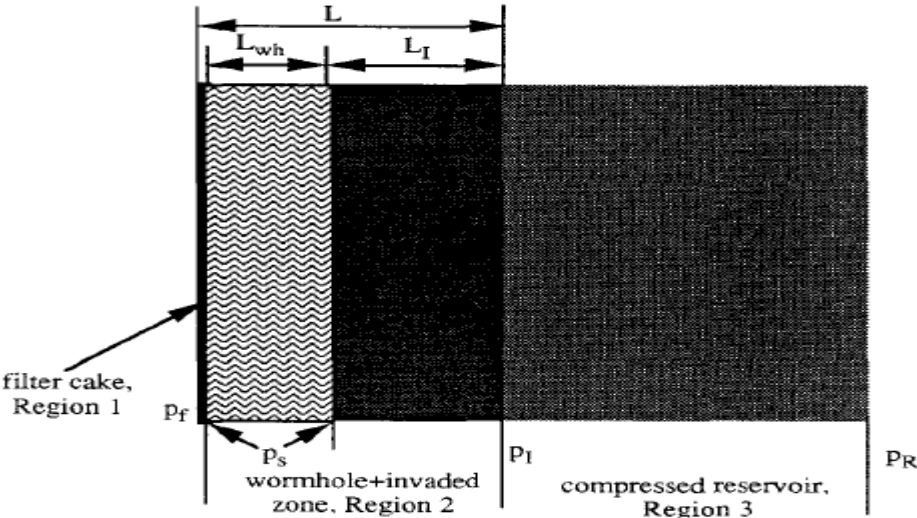
Figure 1.3: Fluid leakoff zones in a fracture face (Hill and Zhu, 1995).

1.3 Research Objectives

An acid fracturing simulator that uses a 3D solution of velocity, pressure, and concentration profiles has already been developed. The approach and algorithm of this simulator is illustrated by Mou (2010) and an analytical validation and some development of the model has been presented by Oeth (2013). The correlation used to evaluate acid fracture conductivity was theoretically developed by Deng et al. (2012). The main objectives of my research are as follows:

1- Provide a detailed study of the algorithm and equations used in the simulator to make it convenient for other researchers to further develop the simulator.

2- Use the simulator to perform parametric studies to evaluate the effect of fluids and formation properties on fracture conductivity and acid penetration distance. The simulator output is imported to the ECLIPSE ™ reservoir simulator to evaluate production enhancement for different cases and to be able to draw a solid conclusion about fracture treatment performance.

3- Provide a summary of simulator limitations and identify other hydraulic, mechanical, thermal, and geochemical phenomena that should be included to improve the model's accuracy. Some input data cause the simulator to prematurely terminate without completing the run. This issue is further investigated in this research.

CHAPTER II

MODEL THEORETICAL APPROACH

2.1 Model Algorithm

The goal of this simulator is to provide conductivity distribution of a fracture after treatment with an acid system. The simulator goes through various steps before providing fracture conductivity distribution. Some steps are performed only once during simulation and others are repeated at each time step. Figure 2.1 shows the simulator's first steps that will not be revisited again during the simulation procedure.
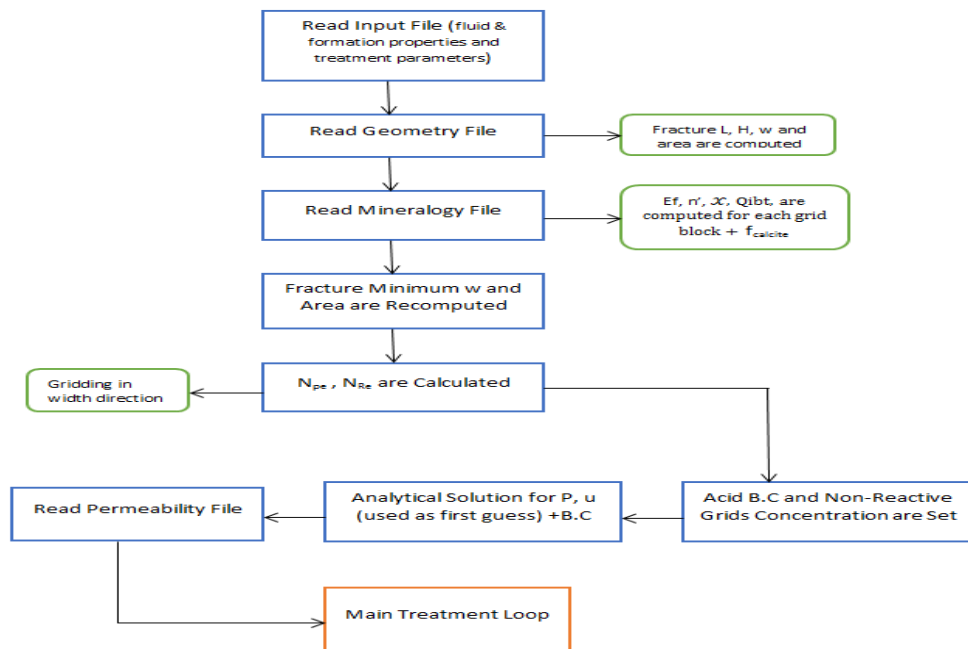
Figure 2.1: Simulator step one algorithm that is performed only one time.

The user has to provide input data that includes fluid and formation properties in addition to treatment parameters. The simulator then reads the fracture width distribution (geometry), which has to be provided by other hydraulic propagation models. The number of grids in the fracture height and fracture length depends on the precision of width distribution provided by the gridding system of the fracture propagation model. Fracture height and length are considered to be constant while fracture width will change during the acid injection. Formations can consist of calcite, dolomite, and nonreactive minerals. The simulator reads mineralogy distribution and computes the reaction rate constant, order of reaction, volume dissolving power, and the pore volume to breakthrough value for each grid cell. The percentage of calcite in a fracture is evaluated and used in the Mou-Deng (2012) conductivity correlation. Fracture average width and area are calculated again where nonreactive grids are excluded this time. Gridding in the width direction is performed by calculating the Peclet number (N_{pe}) and based on that value, the number of grids are determined. The simulator imposes the restriction that the concentration at the fracture inlet and at the nonreactive grid cells is equal to the initial concentration and will not change during treatment. Before moving to the Navier-Stokes and continuity equations, an analytical solution for velocity in the length direction (u_x) and pressure is provided as a first-guess solution. Before moving to main treatment loop, the simulator reads permeability distribution, which affects the fracture leakoff properties.

The main treatment loop is performed at each time step until reaching the end of treatment time (Fig. 2.2). The leakoff coefficient for each gird cell at the fracture face is

calculated by using the two models. As long as the acid front is beyond the grid blocks in the fracture face, the leakoff coefficient without the wormhole effect is considered; otherwise, the wormhole effect should be included. Leakoff velocity through the fracture walls can be estimated and penetration distance afterward can be easily determined. The leakoff velocity is considered as a velocity boundary condition in the width direction (v_y) and can change at each time step. Subsequently, the simulator moves to the continuity and momentum balance equations (Navier-Stokes) to solve for velocity and pressure in 3D. The following steps are performed when the simulator reaches this point (Oeth, 2013):

1) Begin with a guessed velocity profile.

2) Calculate the pressure coefficient matrix based on continuity and the momentum balance equations, and solve for pressure by inverting this matrix.

3) Use the three momentum equations to calculate the velocity profile using pressure values in Step 2.

4) Compare the calculated velocity with the guessed velocity, and if the velocity converges, then terminate the solution; otherwise, restart the algorithm with the new velocity profile.

After completing these steps, a 3D pressure and velocity profile inside of the fracture are obtained. The velocity profile at the entrance is used to calculate the inlet injection rate and if it is within 10% of the user-specified injection rate, then the simulator moves to the acid concentration profile; otherwise, inlet pressure values will be adjusted and the continuity and momentum balance equations will be evaluated again to obtain a velocity

16

profile that satisfies the inlet injection rate. The velocity profile is used for 3D calculations of the concentration profile inside of the fracture. The concentration profile is used to calculate the amount of acid that diffuses through the fracture wall and the concentration of leaked off fluid. An etching profile for each grid cell at the fracture faces is calculated where diffusion and leakoff are considered to be the only methods to reach the fracture wall. These etching profile and fracture statistical parameters are imported into the Mou-Deng correlation file to evaluate the conductivity distribution. The water flushing effect after acid injection is also included in the simulator where the acid concentration in the flushed zone is assumed to be zero. The results are printed in one minute intervals to show how the solutions change with time. The Tecplot Focus ™ program is used to view the results in 2D and 3D. Figure 2.2 shows the flow chart of the approach.
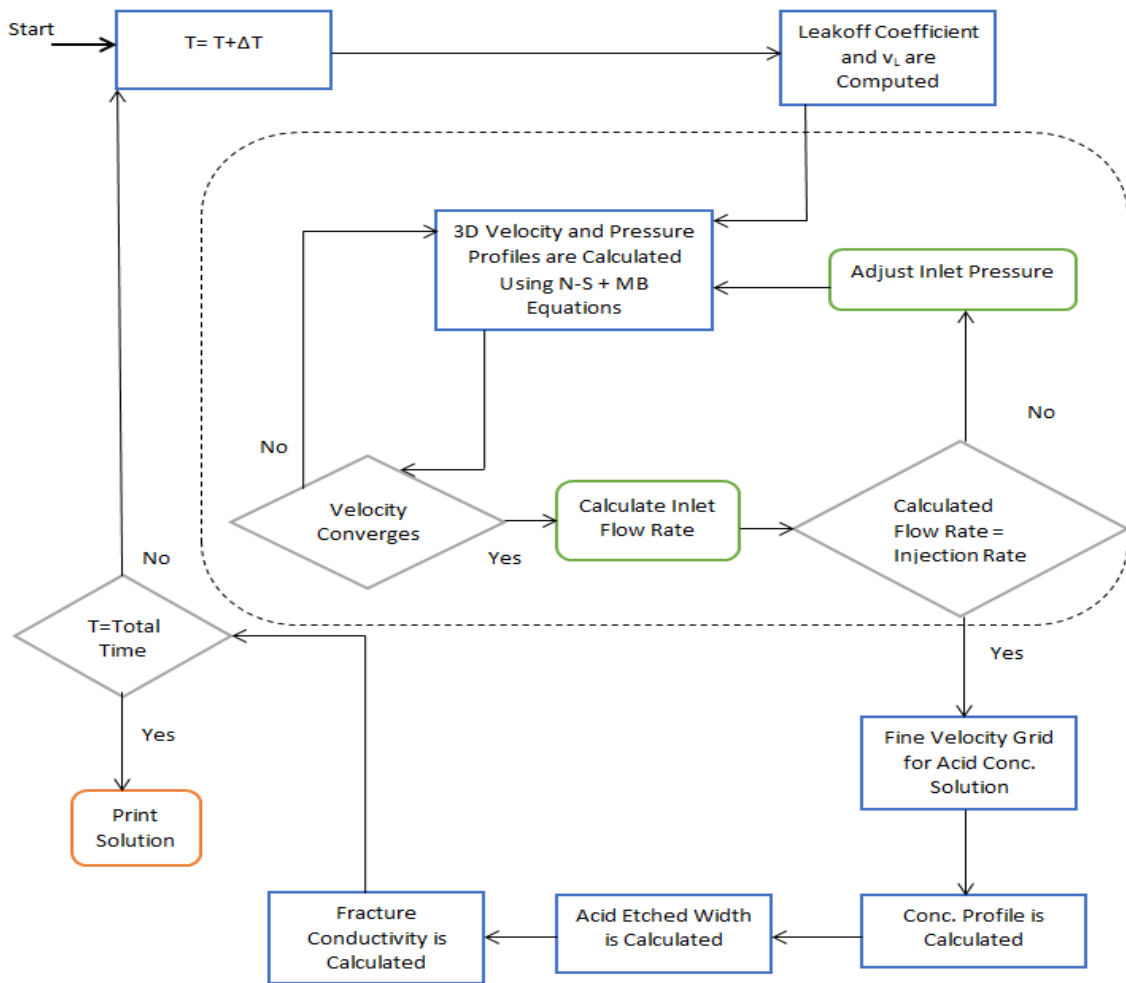
Figure 2.2: The second portion of the simulator algorithm (main loop).

2.2 Model Equations

Some of the equations used in this model are fundamental and based on physics laws such as conservation of mass and momentum. These equations are differential equations and can be solved numerically or analytically. Most of analytical solutions are based on many assumptions and simplifications, which limit the model and cause it to be less representative of the real world. In this model, a numerical solution using SIMPLE (Semi-Implicit Method for Pressure Linked Equations) is implemented where averaging in 1D is no longer needed. This section introduces most of the equations used in the model. For model validation and comparison with analytical solutions, the reader may refer to the Oeth (2013) dissertation.

2.2.1 Reaction Equations

The reaction between an acid and a fracture is heterogeneous where acid has to diffuse to the rock surface to react with the minerals. The diffusion flux (J_y^A) depends on the acid concentration gradient ($\frac{\partial c_A}{\partial y}$) and the diffusion coefficient (D_A) as expressed by Fick's law (Eq.2.1).

$$J_y^A = -D_A \frac{\partial c_A}{\partial y} \dots\dots\dots\dots\dots\dots\dots\dots\dots\dots\dots\dots\dots\dots\dots\dots\dots\dots\dots (2.1)$$

If diffusion is slow when compared with the reaction rate, it becomes the rate determining step and the reaction is called diffusion limited. If the diffusion is faster than the reaction rate, then reaction becomes the rate determining step and the reaction is called reaction limited. Because HCl reactions are so fast, once the molecules collide

with each other, a product will form; hence, an acid reaction, which in this case is diffusion limited.

The reaction rate (Eq. 2.2) depends on the reactant's concentration (C_{HCl}), reaction rate constant (E_f), and the reaction order (α). Because minerals are solid, their concentration will not change and this is not shown in the equation. The reaction rate constant (Eq.2.3) is a function of temperature (T) and the activation energy (ΔE). Lund et al. (1975) studied the reaction between HCl and dolomite and HCl and calcite minerals and summarized the reaction kinetic constants as shown in Table 2.1.

$$-r_{HCl} = E_f C_{HCl}^{\alpha} \ldots\ldots\ldots\ldots\ldots\ldots\ldots\ldots\ldots\ldots\ldots\ldots\ldots\ldots\ldots\ldots\ldots\ldots\ldots\ldots \quad (2.2)$$

$$E_f = E_f^0 \exp(-\frac{\Delta E}{RT}) \ldots\ldots\ldots\ldots\ldots\ldots\ldots\ldots\ldots\ldots\ldots\ldots\ldots\ldots\ldots\ldots\ldots\ldots\ldots \quad (2.3)$$

Table 2.1: Reaction kinetics constants for the reaction between HCl-Calcite and HCl-Dolomite.

Mineral	α	$E_f^0 [\dfrac{kg\ moles\ HCl}{m^2-s-\left(kg-moles\,\frac{HCl}{m^3}\right)^{\alpha}}]$	$\dfrac{\Delta E}{R}$ (K)
Calcite	0.63	$7.55*10^3$	$7.314*10^7$
Dolomite	$\dfrac{6.32*10^{-4}T}{1-1.92*10^{-3}T}$	$7.9*10^3$	$4.48*10^5$

A less complicated way to calculate the amount of etching is by calculating the dissolving power ($\mathcal{X}$) introduced by Williams, Gidley, and Schechter (1979). This calculation is based on the assumption that the reaction between an acid and a mineral is complete. Gravimetric dissolving power (β) should be calculated first (Eq. 2.4), which depends on the stoichiometric coefficient (ν) and molecular weight (MW) of the reactants. The stoichiometric coefficients in this case can be computed by balancing the reaction between the HCl and the minerals (Eq. 2.6-2.7). When the acid concentration is less than 100%, then this concentration should be multiplied by β. By calculating the dissolving power, computing the volume of acid needed to dissolve a certain amount or volume of minerals becomes easy. Weak acids are treated differently because they do not react completely; hence, knowledge of equilibrium composition is inevitable.

$$\beta = \frac{\nu_{mineral}\, MW_{mineral}}{\nu_{acid}\, MW_{acid}} \dots\dots\dots\dots\dots\dots\dots\dots\dots\dots\dots\dots\dots\dots\dots\dots\dots\dots\dots\dots\dots\dots\ (2.4)$$

$$\mathcal{X} = \beta\left(\frac{MW_{acid}}{\rho_{mineral}}\right) \dots\dots\dots\dots\dots\dots\dots\dots\dots\dots\dots\dots\dots\dots\dots\dots\dots\dots\dots\ (2.5)$$

$$2HCl + CaCO_3 \rightarrow CaCl_2 + CO_2 + H_2O \dots\dots\dots\dots\dots\dots\dots\dots\dots\dots\dots\dots\dots\ (2.6)$$

$$4HCl + CaMg(CO_3)_2 \rightarrow CaCl_2 + MgCl_2 + 2CO_2 + 2H_2O \dots\dots\dots\dots\dots\dots\dots\ (2.7)$$
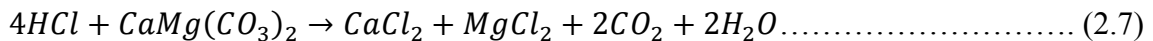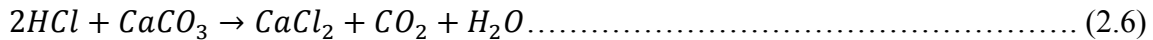
2.2.2 Analytical Solutions for Pressure and Velocity inside the Fracture

Before numerically solving for velocity and pressure in 3D, a first- supposition analytical solution is used. This solution (Eq.2.8) is obtained by simplifying momentum and continuity equations into a 1D solution for velocity. This solution is applied for both Newtonian fluids and non-Newtonian fluids that follow the power low model (Eq.2.11),

where K is the consistency index and n is power low index. When the power low index is one, the fluid is considered Newtonian, which has constant viscosity. The velocity profile in this case is simplified into Equation 2.9. To obtain the velocity profile (Eq.2.8-2.9), the following assumptions are made:

1) The flow is at a steady-state condition.

2) There are no velocity components in the fracture width ($v_y = 0$) and height ($v_z = 0$) directions.

3) There is no velocity gradient in the height direction $\frac{\partial v_x}{\partial z} = 0$.

4) The gravity acts only in the height direction.

5) The velocity (v_x) is zero at the fracture walls and maximum at the center.

$$v_x(y) = v_x(0)\left[1 - \left(\frac{y}{Y}\right)^{\frac{1+n}{n}}\right] \quad\text{(2.8)}$$

$$v_x(y) = v_x(0)\left[1 - \left(\frac{y}{Y}\right)^{2}\right] \quad\text{(2.9)}$$

$$v_x(0) = \frac{1}{2\mu} * \left(-\frac{\partial p}{\partial x}\right) \quad\text{(2.10)}$$

$$\mu_{app} = K \left(\frac{\partial u}{\partial y}\right)^{n-1} \quad\text{(2.11)}$$

The velocity profiles in this case will be constant in the length direction and will vary only in the width direction with the maximum value at the center and the zero values at the wall surfaces. This profile cannot represent the actual acid fracturing conditions where velocity (v_x) is function of length and height directions. Because the

fracture walls are porous, the velocity component in the width direction (v_y) cannot be ignored; however, this solution can be useful as first deduction and input into the Navier-Stokes equations.

A first conjecture as a solution for pressure is provided by assuming that the pressure gradient is constant along the length direction and there is no pressure gradient in other directions (Eq.2.12). The pressure value at the fracture entrance P_{in} is calculated by using Equation 2.13. This calculated value is then populated to all direction as a first deduction and input into the Navier-Stokes equations.

$$-\frac{\partial P}{\partial x} = \left(\frac{\Delta P}{L}\right) \rightarrow \ P = P_{in} - \Delta P * \frac{x}{L} \ \dots\dots\dots\dots\dots\dots\dots\dots\dots\dots\dots\dots\dots\dots \ (2.12)$$

$$P_{in} = \frac{LK\left[q*\dfrac{1+2n}{2nH*\left(\frac{\tilde{w}}{2}\right)^{\frac{2n+1}{n}}}\right]^{n}}{2} \ \dots\dots\dots\dots\dots\dots\dots\dots\dots\dots\dots\dots\dots\dots \ (2.13)$$

2.2.3 Leakoff Coefficient

The leakoff coefficient calculation is very important in designing hydraulic and acid fracturing processes (Ben-Naceur et al., 1989). The shape of the fracture and the penetration distance are both affected by this value. Also, this value can determine the efficiency of a fracturing job, which is the ratio of the pumped fluids volume to the fracture volume. A high-leakoff coefficient can cause premature job failure because the pressure cannot build up to the fracture pressure. The leakoff coefficient consists of three parameters as shown in Figure 2.3. Effluent viscosity (Cv) represents the first layer of the fracture wall that is formed due to the fluid filtrate that penetrates into the wall's

pores. The second layer exists because of the wall building (Cw) due to the accumulation of fluid filtrate during injection. The third layer represents the reservoir fluid viscosity and compressibility (Cc). The effluent and reservoir fluid coefficients can be calculated from the reservoir and fluid properties (Eq. 2.14-2.15) while the wall buildup coefficient can be determined experimentally (Eq. 2.16). There are several methods available to combine the three coefficients into one leakoff coefficient. One method combines Cv and Cc as shown in Equation 2.17 and compares the value with Cw and the lesser coefficient is used as total coefficient. Another method combines the total pressure drop contribution of each coefficient that leads to Equation 2.18. (Recent Advances in Hydraulic Fracturing, 1989)

$$C_v = 0.0469 \left(\frac{k_i \Delta P \varphi}{\mu_a}\right)^{\frac{1}{2}} \quad \dots\dots\dots\dots\dots\dots\dots\dots\dots\dots\dots\dots\dots\dots\dots\dots\dots\dots\dots\dots\dots\dots \quad (2.14)$$

$$C_c = 0.0374 \, \Delta P \left(\frac{k_r C_t \varphi}{\mu_f}\right)^{\frac{1}{2}} \quad \dots\dots\dots\dots\dots\dots\dots\dots\dots\dots\dots\dots\dots\dots\dots\dots\dots\dots\dots\dots \quad (2.15)$$

$$C_w = 0.0164 \frac{k_f A \Delta P}{\mu_f F_{cv}} \quad \dots\dots\dots\dots\dots\dots\dots\dots\dots\dots\dots\dots\dots\dots\dots\dots\dots\dots\dots\dots\dots \quad (2.16)$$

$$C_{vc} = \frac{2 C_v C_c}{C_v + (C_v^2 + 4 C_c^2)^{\frac{1}{2}}} \quad \dots\dots\dots\dots\dots\dots\dots\dots\dots\dots\dots\dots\dots\dots\dots\dots\dots\dots\dots \quad (2.17)$$

$$C_t = \frac{2 C_v C_c C_w}{C_v C_w + [C_w^2 C_v^2 + 4 C_c^2 (C_v^2 + C_w^2)]^{\frac{1}{2}}} \quad \dots\dots\dots\dots\dots\dots\dots\dots\dots\dots\dots\dots\dots\dots \quad (2.18)$$
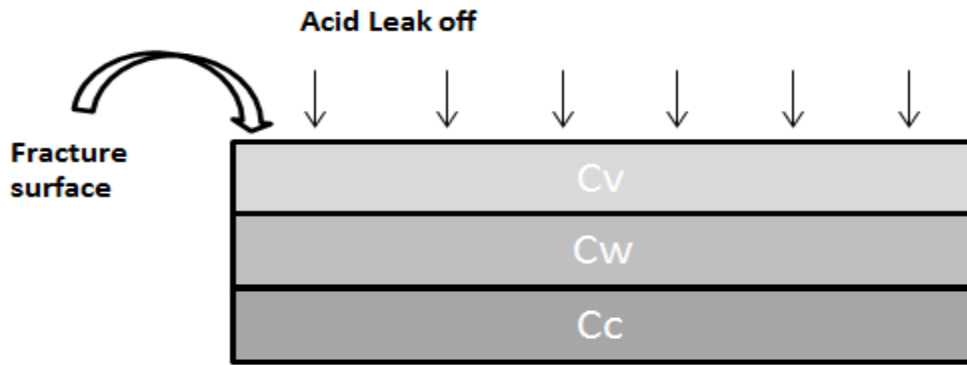
Figure 2.3: Leakoff parameters as it appears in a fracture wall.

Acid injection creates wormholes in fracture walls that affect the leakoff coefficient. The severity of this effect, which depends on the type of formation, is more noticeable in calcite when compared with dolomite formations. This effect can be quantified by measuring the number of pore volumes of acid needed for the wormhole to breakthrough. In this simulator, the value of pore volume to breakthrough (Qibt) for calcite is 1.5 and 20 for dolomite. Then, the Cv value is corrected for the wormhole effect as shown in Equation 2.19. Under the assumption that Cw is large when compared with Cv or Cc, the total leakoff coefficient, including wormhole effect, is shown in Equation 2.20 (Hill and Zhu, 1995).

$$C_{v,wh} = \sqrt{\frac{Q_{ibt}}{Q_{ibt}-1}} * C_v \quad \text{..} \quad (2.19)$$

$$C_t = \frac{-\frac{1}{c_c} + \sqrt{\frac{1}{c_c^2} + \frac{4}{c_{v,wh}^2}}}{2 * \left(\frac{1}{c_{v,wh}^2}\right)}$$ .... (2.20)

The leakoff velocity at the fracture wall is calculated (Eq.2.21) and used as a boundary condition later in Navier-Stokes equations. By volume balance (volume injected = leakoff volume), the penetration distance can be determined using Equation 2.22. After this distance, there is no acid convection or diffusion, which means this part, will have zero conductivity after fracture closure.

$$v_L = \frac{C_t}{\sqrt{t}}$$ .... (2.21)

$$L = \frac{q}{4Hv_L}$$ .... (2.22)

2.2.4 Navier Stokes Equations

To solve for three velocity components (v_x, v_y, v_z) and pressure (P) inside the fracture, four equations are need. These equations are three momentum balances in each coordinate (Eqs. 2.24-2.26) and one continuity equation (Eq.2.23). These equations are further simplified by making the following assumptions:

1) A steady-state condition exists, which means no property change will occur with time $\frac{\partial(\rho, v_x, v_y, v_z)}{\partial t} = 0$.

2) Newtonian fluids are assumed for these equations, but the model can handle non-Newtonian fluids as well (Oeth, 2013).

3) Gravity effect is neglected ($\rho g = 0$).

4) Density is constant (incompressible fluid).

$$\frac{\partial \rho}{\partial t} + \frac{\partial(\rho v_x)}{\partial x} + \frac{\partial(\rho v_y)}{\partial y} + \frac{\partial(\rho v_z)}{\partial z} = 0 \ldots\ldots\ldots \text{(2.23)}$$

$$\rho \left(\frac{\partial v_x}{\partial t} + v_x \frac{\partial v_x}{\partial x} + v_y \frac{\partial v_x}{\partial y} + v_z \frac{\partial v_x}{\partial z} \right) = -\frac{\partial p}{\partial x} + \mu \left(\frac{\partial^2 v_x}{\partial x^2} + \frac{\partial^2 v_x}{\partial y^2} + \frac{\partial^2 v_x}{\partial z^2} \right) + \rho g_x \ldots\ldots \text{(2.24)}$$

$$\rho \left(\frac{\partial v_y}{\partial t} + v_x \frac{\partial v_y}{\partial x} + v_y \frac{\partial v_y}{\partial y} + v_z \frac{\partial v_y}{\partial z} \right) = -\frac{\partial p}{\partial y} + \mu \left(\frac{\partial^2 v_y}{\partial x^2} + \frac{\partial^2 v_y}{\partial y^2} + \frac{\partial^2 v_y}{\partial z^2} \right) + \rho g_y \ldots\ldots \text{(2.25)}$$

$$\rho \left(\frac{\partial v_z}{\partial t} + v_x \frac{\partial v_z}{\partial x} + v_y \frac{\partial v_z}{\partial y} + v_z \frac{\partial v_z}{\partial z} \right) = -\frac{\partial p}{\partial z} + \mu \left(\frac{\partial^2 v_z}{\partial x^2} + \frac{\partial^2 v_z}{\partial y^2} + \frac{\partial^2 v_z}{\partial z^2} \right) + \rho g_z \ldots\ldots \text{(2.26)}$$

Boundary conditions are needed to solve the differential equations, and these boundary conditions are as follows:

1) At the inlet, the injection rate must be equal to the summation of volumetric flux across the fracture inlet area.

$$q_{in} = \int v_{x|x=0} dA \ldots\ldots\ldots \text{(2.27)}$$

2) At the outlet, the pressure at the end of fracture is equal to outlet pressure.

$$p_{|x=L} = p_{out} \ldots\ldots\ldots \text{(2.28)}$$

3) On the fracture surfaces, the velocity component in the fracture length and height directions are zero but the velocity in the width direction is equal to leakoff velocity.

$$v_{x|y=y1,y2} = 0 \ldots\ldots\ldots \text{(2.29)}$$

$$v_{z|y=y1,y2} = 0 \ldots\ldots\ldots \text{(2.30)}$$

$$v_{y|y=y1,y2} = v_L \ldots\ldots\ldots \text{(2.31)}$$

4) At the top and bottom of the fracture, all velocity components are equal to zero.

$$v_x, v_y, v_z{}_{|z=0,H} = 0 \dots\dots\dots\dots\dots\dots\dots\dots\dots\dots\dots\dots\dots\dots\dots\dots\dots\dots \text{(2.32)}$$
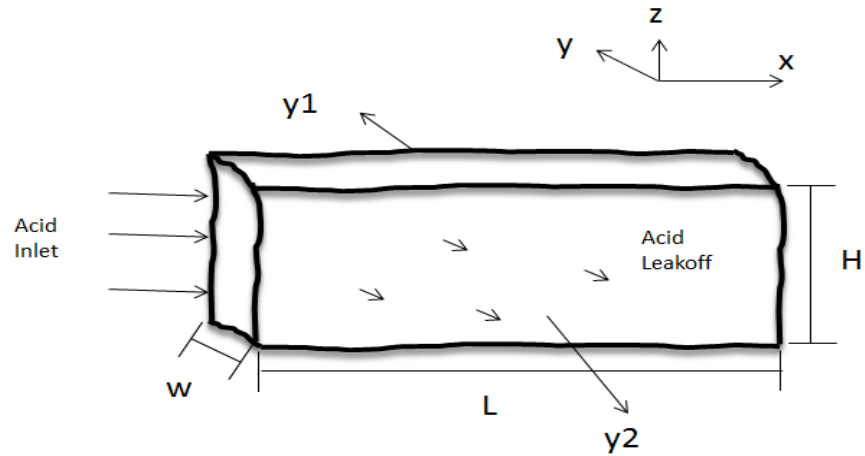
Figure 2.4: Fracture physical domain.

During acid injection, the physical domain (Fig. 2.4) of the fracture changes continuously because the rock is dissolving. This phenomenon causes difficulty in imposing boundary conditions when solving the equations numerically. A front fixing method (Crank 1984) is used to handle this problem where a fixed computational domain is used. For additional information about this topic, the reader may refer to Mou (2010).

2.2.5 Acid Balance Equation and Etched Width Calculation

Solving the mass balance equation (Eq. 2.33) for acid will provide the concentration profile in 3D when convection in all directions is assumed. The velocity profile from the Navier-Stokes equations is used as input into the acid balance equation. Diffusion is assumed to be only in the width direction where diffusion in other directions is neglected. In this case, the acid concentration is a function of time and space.

$$\frac{\partial C_A}{\partial t} + v_x \frac{\partial C_A}{\partial x} + v_y \frac{\partial C_A}{\partial y} + v_z \frac{\partial C_A}{\partial z} = \frac{\partial}{\partial y}\left(D_{eff} \frac{\partial C_A}{\partial y}\right) \dots\dots\dots\dots\dots\dots\dots\dots\dots \quad (2.33)$$

The following boundary conditions are implemented to solve for acid mass balance numerically:

1) Initial condition, at t = 0, there is no acid inside the fracture.

$$C_A(x, y, z, 0) = 0 \dots\dots\dots\dots\dots\dots\dots\dots\dots\dots\dots\dots\dots\dots \quad (2.34)$$

2) At the inlet, the acid is live and no reaction has begun.

$$C_A(0, y, z, t) = C_i \dots\dots\dots\dots\dots\dots\dots\dots\dots\dots\dots\dots \quad (2.35)$$

3) At the top and bottom, no acid concentration gradient is assumed.

$$\frac{\partial C_A}{\partial z}\Big|_{z=0,H} = 0 \dots\dots\dots\dots\dots\dots\dots\dots\dots\dots\dots\dots \quad (2.36)$$

4) At the fracture surfaces, the rate of acid diffusion is equal to the rate of the acid reaction.

$$D_{eff} \frac{\partial C_A}{\partial y} = E_f\left(C_A - C_{eqm}\right)^n (1 - \varphi)\big|_{y1,y2} \dots\dots\dots\dots\dots\dots\dots \quad (2.37)$$

Solving the concentration profile will provide the acid concentration that will react with fracture minerals. There are two methods for transporting the acid to the

fracture walls: 1) Acid leakoff to the fracture ($v_L C_A$); 2) Acid diffusing flux into the

fracture walls because of the acid gradient ($D_{eff} \frac{\partial C_A}{\partial y}$). By the end of this step, the amount

of acid that will react with minerals at each part of fracture walls will be known and its

concentration at each time step is obtained. The next step is to evaluate the amount of

rock dissolved and update the fracture width at each grid block. A volumetric dissolving

power concept is used to evaluate the volume of rock etched as given in Equation (2.38).

In this equation, the rate of width change is represented by this term ($\frac{\partial y(x,z,t)}{\partial t}$), while

the fraction of acid that will react after leakoff is represented by (f). Evaluating this

fraction can be accomplished by laboratory measurements of the acid concentration of

the leaked off acid.

$$\frac{\partial y(x,z,t)}{\partial t} = \frac{\beta MW_{acid}}{\rho(1-\varphi)} \left(f v_L C_A - D_{eff} \frac{\partial C_A}{\partial y} \right) \quad \text{..} \quad (2.38)$$

2.2.6 Conductivity Calculation (Mou-Deng Correlation)

      Mou and Deng (2012) used an exponential function (Eq. 2.39) to correlate

fracture conductivity (wk_f) with closure stress (σ_c). This is the same model used by

Nierode-Kruck (1973) but the constants (α, β) are determined using a large number of

numerical experiments. To determine these constants, three cases are discussed:

$$wk_f = \alpha e^{-\beta \sigma_c} \quad \text{..} \quad (2.39)$$

    1) Dominant permeability distribution

      In this case, the mineralogy distribution is assumed to be moderately

homogenous but the leakoff coefficient is assumed to be greater than 0.004 ft/(min)$^{.5}$ or

approximately 0.001 ft/(min)$^{.5}$. Because the leakoff is high and the minerals are either 100% calcite or 100% dolomite, the permeability effect will prevail. In their correlations, they used the average fracture width $\widetilde{w}$ (Eq.2.40-2.41) instead of the ideal width w_i (rock dissolved volume over fracture area).

$$\widetilde{w} = 0.65 \operatorname{erf}(0.8\sigma_D) w_i^{.83} \quad C_t > 0.004 \text{ ft/(min)}^{1/2} \ldots\ldots\ldots\ldots\ldots\ldots\ldots\ldots\ldots \text{(2.40)}$$

$$\widetilde{w} = 0.2 \operatorname{erf}(0.78\sigma_D) w_i^{.81} \quad C_t \approx 0.001 \text{ ft/(min)}^{1/2} \ldots\ldots\ldots\ldots\ldots\ldots\ldots\ldots \text{(2.41)}$$

To begin with, the conductivity at zero closure stress $(wk_f)_0$ should be evaluated (Eq. 2.42). This value is incorporated into α with other statistical parameters for the permeability distribution ($\lambda_{D,x}, \lambda_{D,z}, \sigma_D$), while Young's modulus (E) is incorporated into β (Eqs. 2.43-2.44).

$$(wk_f)_0 = 4.48 * 10^9 \widetilde{w}^3 \left[1 + \left(a_1 \operatorname{erf}\left(a_2(\lambda_{D,x} - a_3) \right) - a_4 \operatorname{erf}\left(a_5(\lambda_{D,z} - a_6) \right) \right) \sqrt{e^{\sigma_D} - 1} \right],$$

$a_1 = 1.82, \ a_2 = 3.25, \ a_3 = 0.12, \ a_4 = 1.31, \ a_5 = 6.71, \ a_6 = 0.03$ ....… (2.42)

$$\alpha = (wk_f)_0 \left[0.22(\lambda_{D,x}\sigma_D)^{2.8} + 0.01\left((1 - \lambda_{D,z})\sigma_D \right)^{0.4} \right]^{.52} \ldots\ldots\ldots\ldots\ldots\ldots \text{(2.43)}$$

$$\beta = [14.9 - 3.78 \ln(\sigma_D) - 6.8 \ln(E)] * 10^{-4} \ldots\ldots\ldots\ldots\ldots\ldots\ldots\ldots\ldots \text{(2.44)}$$

2) Dominant mineralogy distribution

In this case, the leakoff coefficient is assumed to be less than 0.004 ft/(min)$^{.5}$ and both the dolomite and calcite minerals exist in the formation. The percentage of calcite is needed in the correlation while the permeability distribution statistical parameters are no longer used in the correlations (Eqs. 2.45-2.47).

$$(wk_f)_0 = 4.48 * 10^9 [1 + 2.97(1 - f_{calcite})^{2.02}][0.13 f_{calcite}^{0.56}]^3 w_i^{2.52} \quad \ldots\ldots\ldots\ldots\ldots (2.45)$$

$$\alpha = (wk_f)_0 (0.811 - 0.853 f_{calcite}) \quad \ldots\ldots\ldots\ldots\ldots\ldots\ldots\ldots\ldots\ldots\ldots (2.46)$$

$$\beta = [1.2 e^{0.952\, f\,calcite} + 10.5 E^{-1.823}] * 10^{-4} \quad \ldots\ldots\ldots\ldots\ldots\ldots\ldots\ldots\ldots\ldots\ldots\ldots (2.47)$$

3) Competing between mineralogy and permeability distributions

In this case, the leakoff coefficient is medium; approximately 0.001 ft/(min)$^{.5}$, and both minerals exist in the formation. The conductivity correlations for this case are shown in Equations 2.48–2.50:

$$(wk_f)_0 = 4.48 * 10^9 \left[1 + a_1 + \left(a_2 \operatorname{erf}\left(a_3(\lambda_{D,x} - a_4)\right) - a_5 \operatorname{erf}\left(a_6(\lambda_{D,z} - a_7)\right)\right)\sqrt{e^{\sigma_D} - 1}\right] [a_8 f_{calcite}^{a_9} + a_{10}\sigma_D]^3 w_i^{a_{11}}$$

$$a_1 = 0.2, a_1 = 1.0, \ a_3 = 5.0, a_4 = 0.12, a_5 = 0.6, a_6 = 3.5, a_7 = 0.03, a_8 = 0.1, \ a_9 = 0.43, \ a_{10} = 0.14, \ a_{11} = 2.52 \quad \ldots\ldots\ldots\ldots\ldots\ldots\ldots\ldots\ldots\ldots (2.48)$$

$$\alpha = (wk_f)_0 [0.21 \lambda_{D,x}^{0.16} + 0.046 \ln(\sigma_D) + 0.15 \lambda_{D,z}^{-0.17}] \quad \ldots\ldots\ldots\ldots\ldots\ldots\ldots\ldots (2.49)$$

$$\beta = [53.8 - 4.58 \ln(E) + 18.9 \ln(\sigma_D)] * 10^{-4} \quad \ldots\ldots\ldots\ldots\ldots\ldots\ldots\ldots\ldots\ldots (2.50)$$

CHAPTER III

PARAMETRIC STUDY

The acid fracturing model is constructed to be able to predict the actual behavior of reactive fluids inside of a fracture. Conductivity and penetration distance for various treatment conditions can be obtained from the simulator. The conductivity and penetration distance have a large impact on the production improvement of a fractured well. In this section, different parameters will be tested to detect the effect of each parameter on conductivity and penetration distance. To run the simulator, a fracture domain should be created. In this case, a PKN geometry model is generated and will be used for the majority of the cases. This geometry has an elliptical shape at the wellbore entrance with maximum width at the centerline and zero width at the top and bottom (Fig. 3.1)
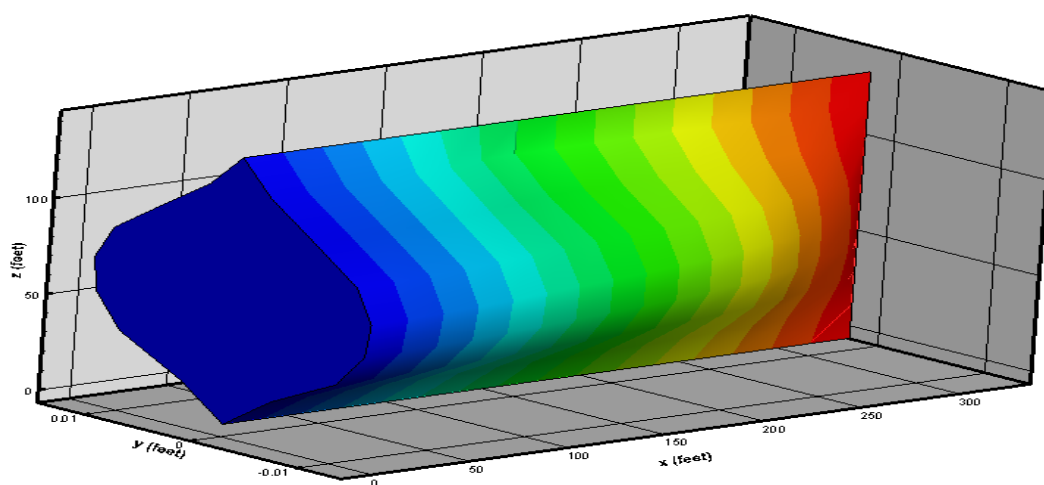

Figure 3.1: A PKN geometry domain.

33

3.1 Acid Type

Different types of acid systems will behave differently inside of the fracture and will provide different results. Straight acid is the simplest type of acid system where no viscosifers or gelling agents are added. Usually, more complex acid systems are used for acid fracturing to improve leakoff efficiency and to make the acid more retarded. In this section, three different types of acid systems are studied: straight, emulsified, and gelled acid. The properties of these fluids are shown in Table 3.1 (De Rozieres et al., 1994).

Table 3.1: Acid system properties used in the simulator.

Acid Type	K (Pa.s^n)	n	D_{eff} (cm^2/s)	μ_a (cp)	T (F)
Straight	0.00109	1.0	0.0000213	1	84
Gelled	0.05	0.65	0.000008	15	84
Emulsified	0.315	0.675	2.64E-08	30	83

The input treatment parameters are shown in Table 3.2 where the mineralogy is assumed to be 100% calcite. Usually, acid fracturing consists of numerous stages of acid and pad fluids injection but for simplification purposes, only one pad stage is assumed to create the fracture and one acid stage to etch the walls of the fracture. The simulator can show the velocity, pressure, concentration, and viscosity profiles in 3D, and it shows acid-etched width and conductivity profiles in 2D.

Table 3.2: Input treatment parameters for the acid fracturing simulator.

Parameters	Value	Unit
Total Compressibility (ct)	.000015	1/psi
Fluid Density (ρ_f)	1070	Kg/m^3
Formation Porosity (φ)	.15	
Temperature (T)	84	F
Limestone Formation Density (ρ_{lim})	2710	Kg/m^3
Fraction of Acid Reaction (f)	.3	
Injection Rate (q_{in})	20	bbl/min
Injection Time	20	min
Wormhole Breakthrough Pore Volume for Limestone (Qibt)	1.5	
Formation Closure Stress (σ_c)	2000	psi
Acid Initial concentration (C_i)	15	wt %
Flush volume	0	bbl
Correlation length ($\lambda_{D,x}$)	1.0	
Correlation length ($\lambda_{D,z}$)	0.05	
Standard deviation	0.4	
Young modulus	4.5	MMpsi

A former version of the simulator could not capture different penetration distances for different fluid systems. For a fracture with a 320-ft half-length, it is unrealistic to expect the straight acid to reach the tip of the fracture as shown in Figure 3.2. A high-leakoff coefficient will not allow the acid to penetrate deep into the fracture. Even if straight acid has a low-leakoff coefficient, it will be mostly consumed at the

fracture entrance because of the high-diffusion coefficient. This error can show that straight acid will result in the best treatment in terms of production enhancement, which contradicts field case results.

It should be mentioned that penetration distance is either fluid-loss limited or reaction-rate limited. To be reaction-rate limited, it is assumed that the pad fluid will control the leakoff rate and the penetration distance is maximum because of the acid consumption. To be fluid-loss limited, the acid will create wormholes that overcome the effect of the pad fluid and result in an excessive leakoff rate, resulting in minimum penetration distance. This case is supported by field data (Nierode and Kruk, 1973) and will be the assumed case in this simulator.
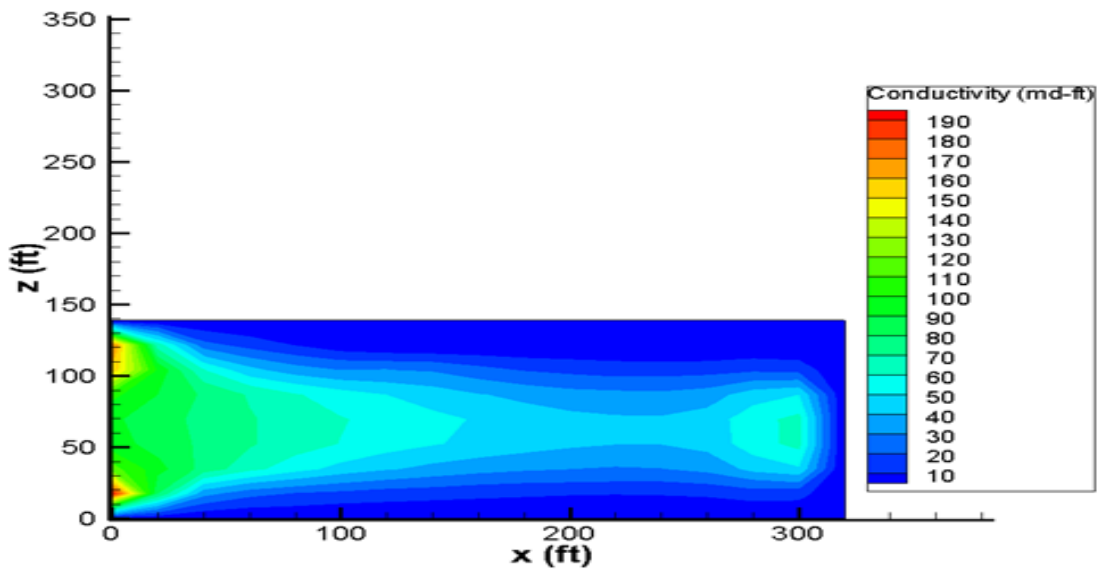
Figure 3.2: Conductivity distribution for straight acid in the fracture (previous simulator version).

3.1.1 Straight Acid

Instead of showing the 3D profile for velocity and concentration profiles, a representative slice in the z-direction will be used. Figure 3.3 shows that the straight acid could not penetrate beyond 120 ft. This penetration distance represents the convection in the length direction (v_x). The contours show that velocity is maximum at the center of the fracture and is zero at the fracture walls. This solution agrees with the analytical solution of the velocity in the x-direction.
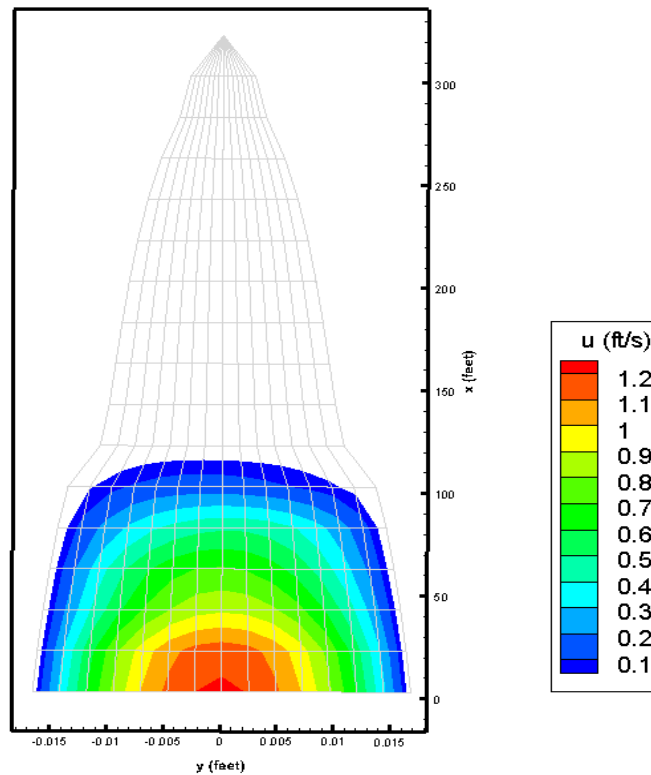
Figure 3.3: Velocity profile (vx) in x-direction for straight acid.

Figure 3.4 shows the velocity profile in the fracture width direction (v_y). Velocity is zero at the center of the fracture and reaches maximum at the fracture walls because of acid leakoff. An analytical solution of velocity in the y-direction with a leaky channel supports this numerical solution. Because of the leakoff effect, the profile reaches up to 120 ft and there is no convection beyond that distance.

Figure 3.5 shows the concentration profile for straight acid where concentration at the inlet and middle of fracture is almost the same as the initial concentration. Toward the fracture walls and at the end of the profile, the concentration decreases but never reaches zero. All of the cases run in the simulator have a Peclet number greater than one, which means that the acid will leakoff before it is consumed completely (fluid loss limit cases).
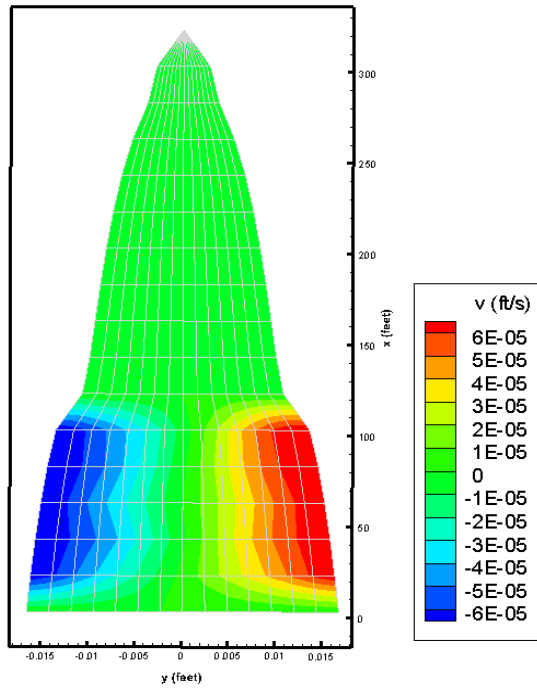
Figure 3.4: Velocity profile (v_y) in y-direction for straight acid.
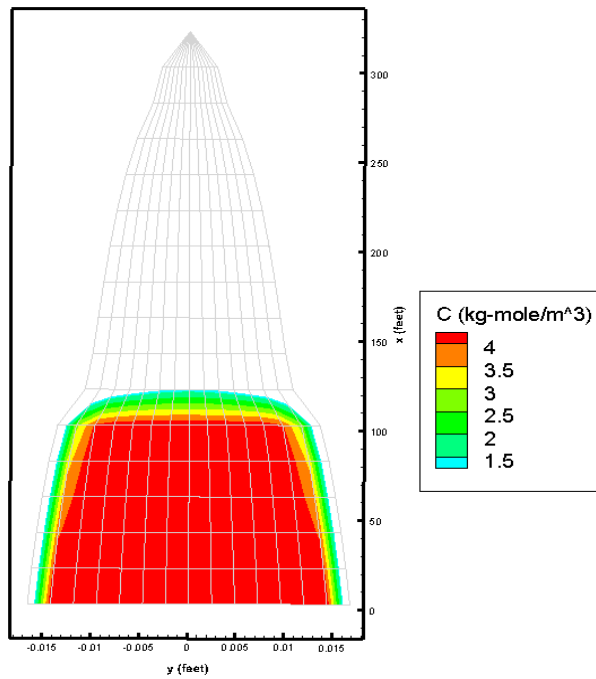
Figure 3.5: Straight acid concentration profile.

39

Rock etching volume is expected to decrease as the acid travel further into the fracture as presented in Figure 3.6. Straight acid has higher etching potential when compared with other fluid systems because of the extremely high diffusion coefficient. However, straight acid is expected to travel less distance inside of the fracture because of the low effluent viscosity, resulting in a higher overall leakoff coefficient; and hence, a higher leakoff rate.
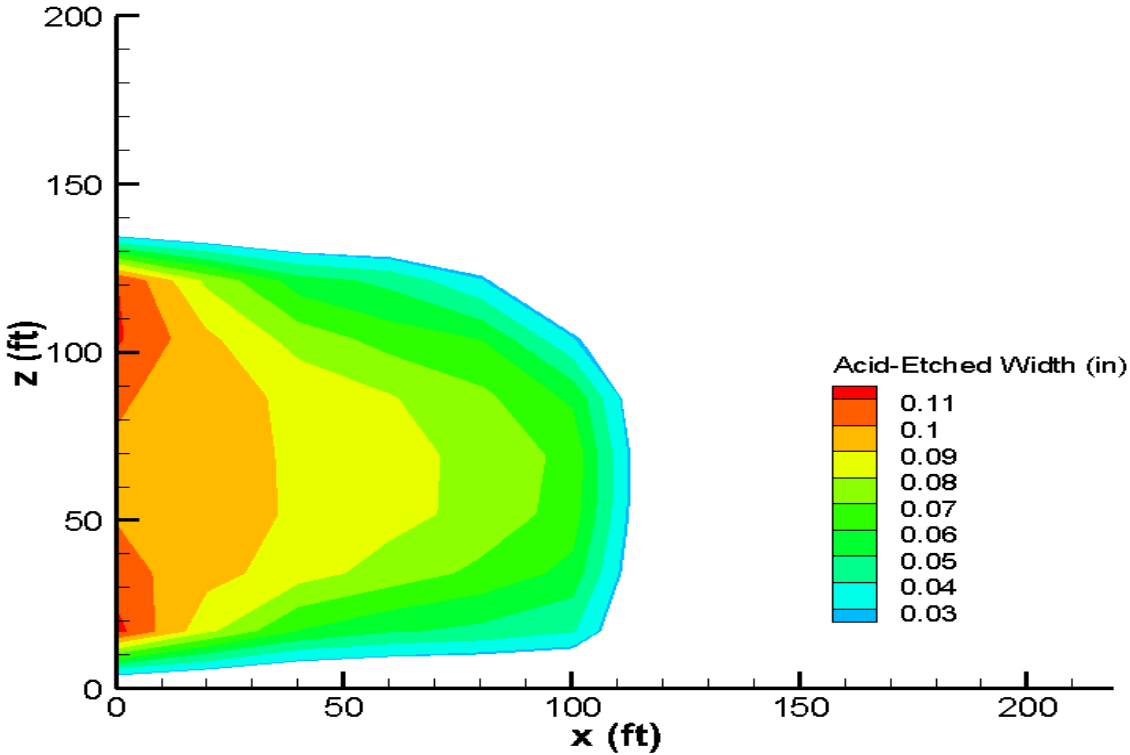
Figure 3.6: Straight acid etched width profile.

40

The conductivity profile usually follows the etching profiles as the Mou-Deng correlation suggest (Fig. 3.7), which means that the higher etched volume zones will have higher conductivity for a given mineralogy and permeability distribution. This condition may not be always correct because of the rock softening effect, not accounted for in most conductivity correlations.
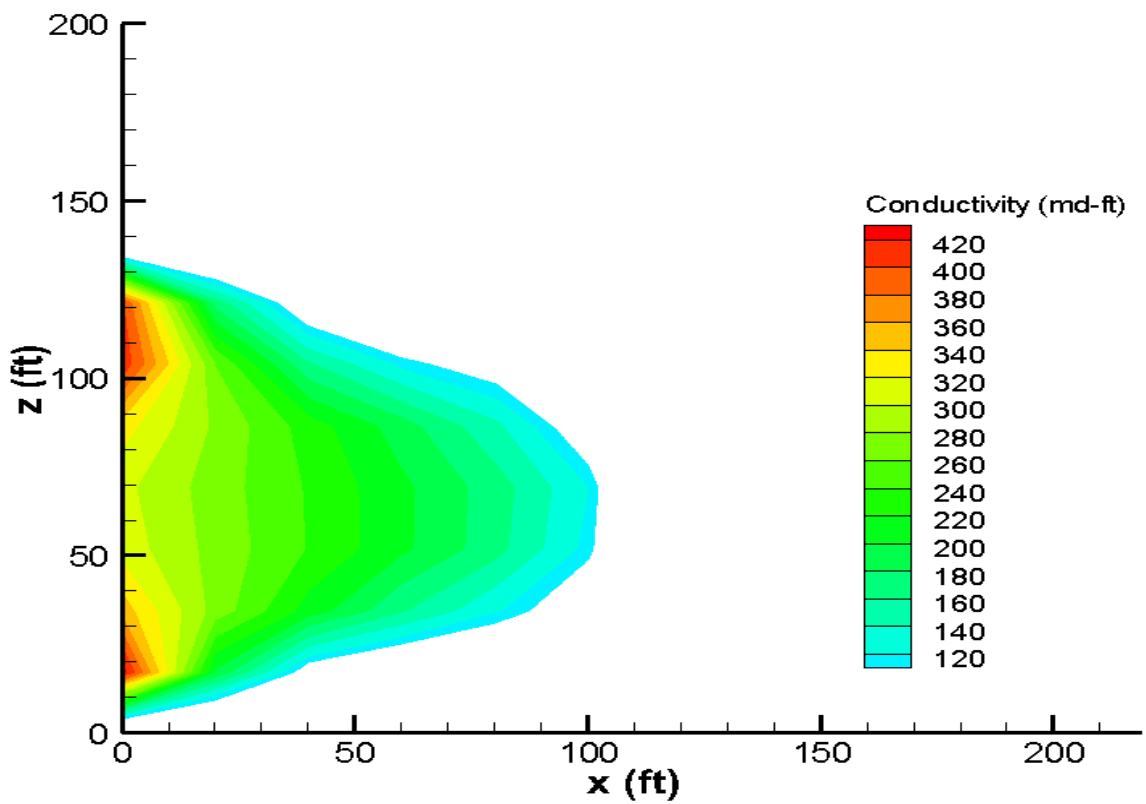
Figure 3.7: Straight acid conductivity profile.

3.1.2 Gelled Acid

Gelled acid is simulated in this case where the gelling agent is added to the HCl. Gelled acid has been used in the industry and proved to be more effective for acid fracturing. Crowe et al. (1981) investigated different gelling agents in terms of stability, efficiency, and condition after spending. The study provided the concentration and temperature at which some gelling agents will be more stable. Also, the potential of various gelling agents was tested in their study where xanthan polymers showed the greatest overall potential. The viscosity of gelled acid is several times greater than the viscosity of straight acid; however, the diffusion coefficient of gelled acid is less than the straight acid diffusion coefficient, which decreases the amount of acid flux to the fracture walls. Laboratory experiments with a gelled acid show a lower etching potential when compared with straight acid etching.. Simulating the gelled acid case showed that the acid convection can reach up to 240 ft inside of the fracture (Fig. 3.8). This penetration distance is almost double the penetration distance of a straight acid, indicating an efficiency improvement in leakoff behavior.
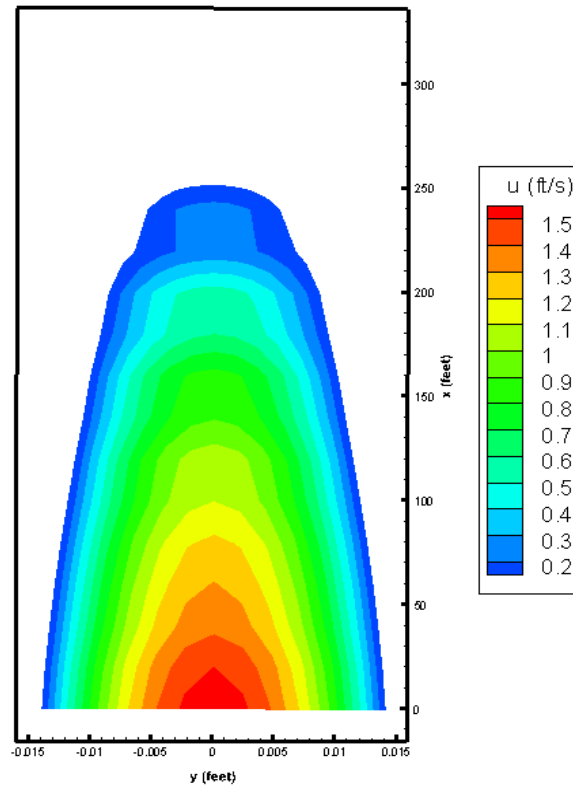
Figure 3.8: Velocity profile (vx) in x-direction for gelled acid.

On the average, the conductivity values for gelled acid are lower than that for straight acid as shown in Figure 3.9 but gelled acid penetrates deeper into the fracture. It can be concluded that gelled acid can be used to etch medium depth fractures (200-300 ft).
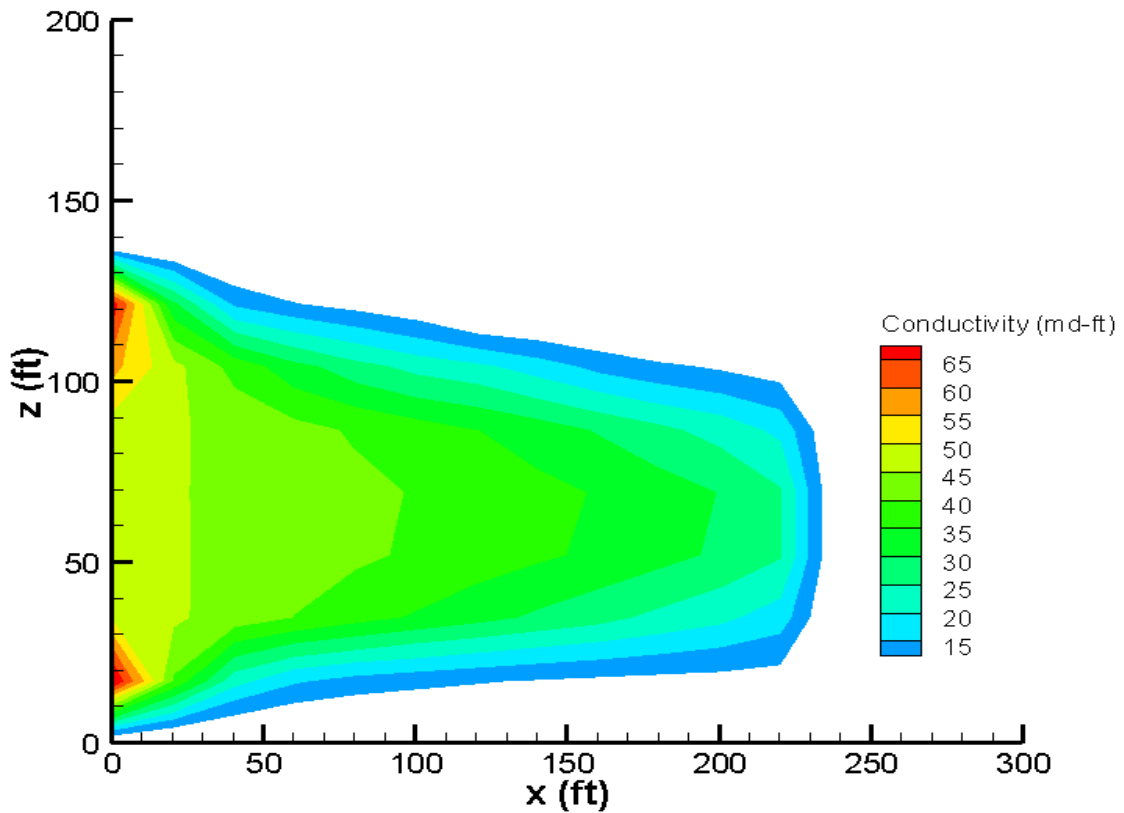
Figure 3.9: Conductivity profile for gelled acid.

3.1.3 Emulsified Acid

Emulsifiers are added to HCl to create emulsified acid that has higher viscosity than that of straight acid. This makes the acid more retarded and helps control the leakoff rate by reducing the leakoff coefficient. However, the etching potential is reduced because of the low-diffusion coefficient and leakoff rate, which means less acid will react with the fracture walls. Other effects may be observed in the production stage such as an additional pressure drop because of the skin developed due to high-viscosity filtrate. This phenomenon is known as viscous skin and it is more pronounced in a gas

reservoir. Simulating emulsified acid shows that acid can reach up to the tip of the

fracture (320 ft) as shown in Figure 3.10.
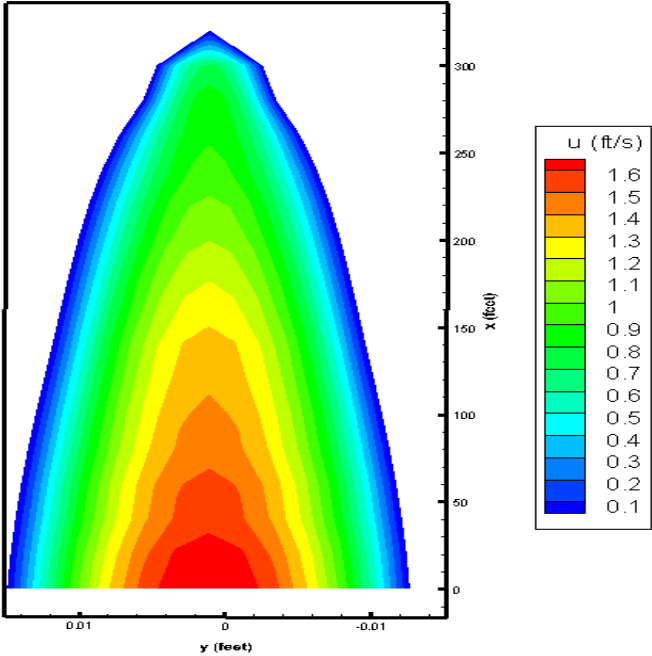
Figure 3.10: Velocity profile (vx) in x-direction for emulsified acid.
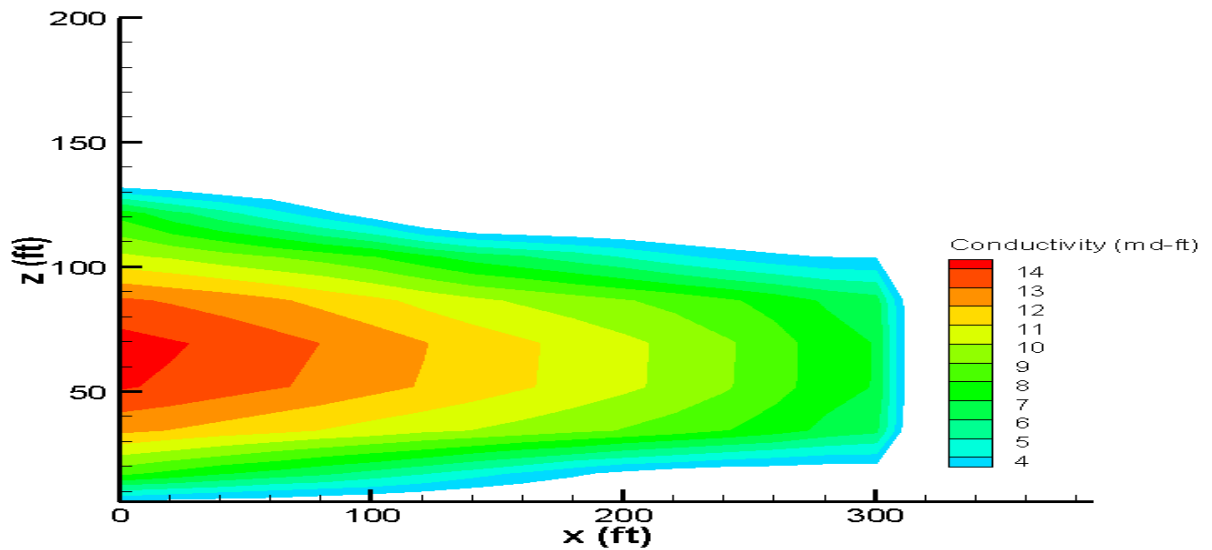
Figure 3.11: Conductivity profile for gelled acid.

The conductivity profile shows an enhanced homogenous conductivity distribution when compared with straight or gelled acids (Fig. 3.11). This effect is evident in acids with low-diffusion coefficients. It is observed that emulsified acid can reach lengthy distances inside of fractures, which makes it a good candidate for very long fractures. Figure 3.12 shows conductivity along the fracture length for the three acid systems. The straight acid has a very high conductivity at the fracture entrance, but it drops to zero very quickly. Gelled acid has lower conductivity than straight acid but it penetrates deeper into the fracture. Emulsified acid has the lowest conductivity but has the greatest penetration. To measure the effect of these three treatments on the production, files are imported into the ECLIPSE reservoir simulator.
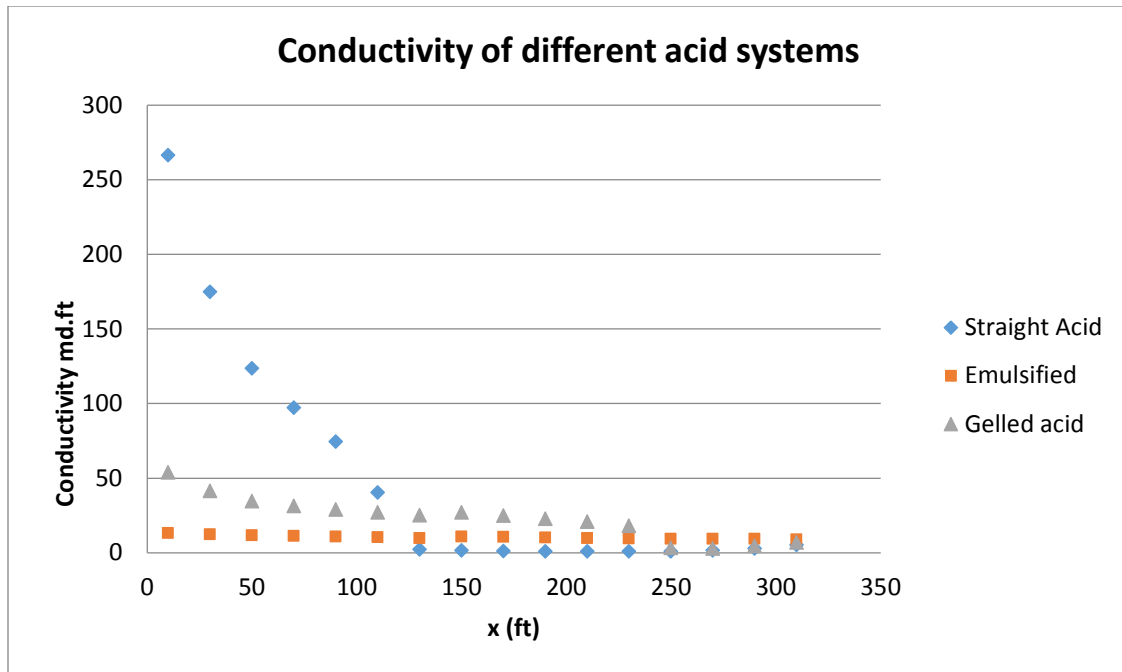
Figure 3.12: Conductivity versus distance for straight, emulsified and gelled acids.

3.1.4 ECLISPE Simulation

Production rate enhancement after acid fracturing is a measurement of treatment

success. Certain reservoir properties are assumed when simulating the three acid

fracturing cases as shown in Table 3.3. The vertical fracture is assumed to be in the

middle of the reservoir where perforations are considered along the fracture height (Fig.

3.13). A constant bottomhole pressure at 1,500 psi is assumed to be the pressure during

production. Dead oil properties are implemented and a water aquifer is assumed to

underlay the oil formation. The conductivity distribution for each case is imported to the

ECLISPE simulator where the production rate and cumulative oil production for 480

days are simulated. Different values of reservoir permeability are considered to capture

the effect of each acid system in permeable and tight formations.

Table 3.3: Reservoir properties for the three acid fracturing cases.

Reservoir properties		
φ	0.15	
Lx	1870	ft
Ly	1556	ft
H	230	ft
H perf	140	ft
P	2900	psi
Depth	6505	ft
oil ρ	41.9	lbm/ft^3
μ	0.0879	cp
rw	0.365	ft
skin	0	
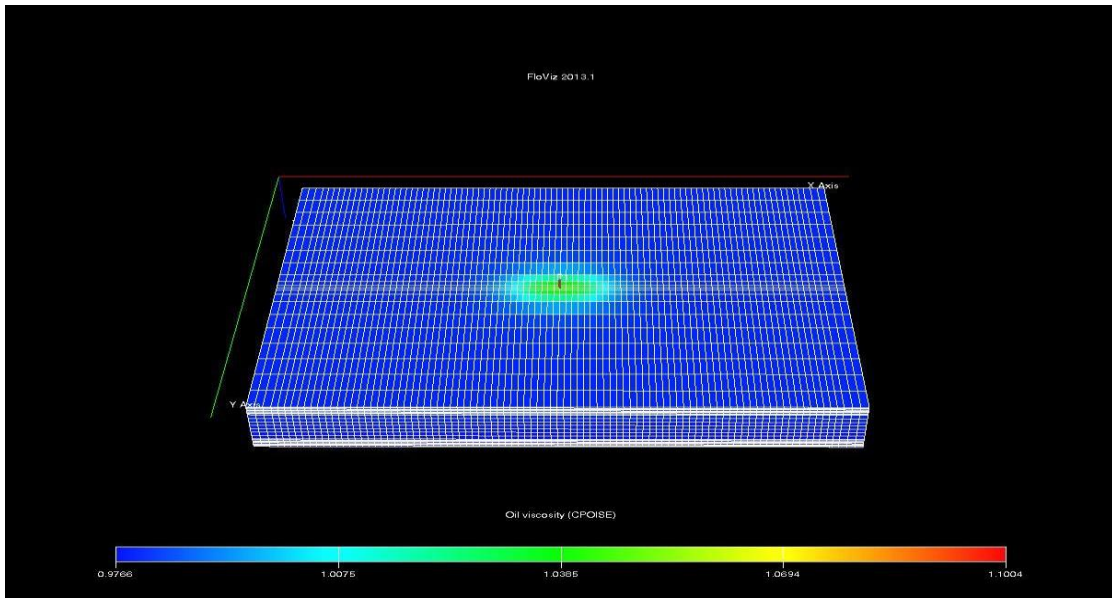
Figure 3.13: Visualization of the reservoir geometry and the well and fracture locations.

From Figure 3.14, the production rate from the reservoir with a gelled-acid fracture treatment begins with a transient period for approximately 100 days. During this period, the production rate is reasonable starting at 1100 bbl/day but it drops rapidly to 400 bbl /day after 100 days. After that, the pressure drawdown reaches the reservoir boundaries, and the production rate follows a pseudo steady-state condition where production decreases steadily to approximately 240 bbl/day. The different cases show similar behavior but with different flow rates. Cumulative oil production for the entire period is shown in Figure 3.15. This value and the dimensionless fracture conductivity (Eq.3.1) will be used to compare all of the simulated cases. Researchers showed that there is an optimum value for dimensionless fracture conductivity that will optimize the productivity index, which is on the order of 1.6 (Cinco-Ley and Samaniego, 1981). This

49

result implies that for a given formation with a specific permeability, there is a fracture

half-length and conductivity that will maximize the productivity index. Dimensionless

conductivity and productivity index are as follows:

$$C_{fD} = \frac{k_f w}{k x_f} \quad \dots\dots\dots\dots\dots\dots\dots\dots\dots\dots\dots\dots\dots\dots\dots\dots\dots\dots\dots\dots\dots\dots\dots\dots\dots\dots \text{(3.1)}$$

$$J = \frac{q}{\Delta p} \quad \dots\dots\dots\dots\dots\dots\dots\dots\dots\dots\dots\dots\dots\dots\dots\dots\dots\dots\dots\dots\dots\dots\dots\dots\dots\dots\dots \text{(3.2)}$$
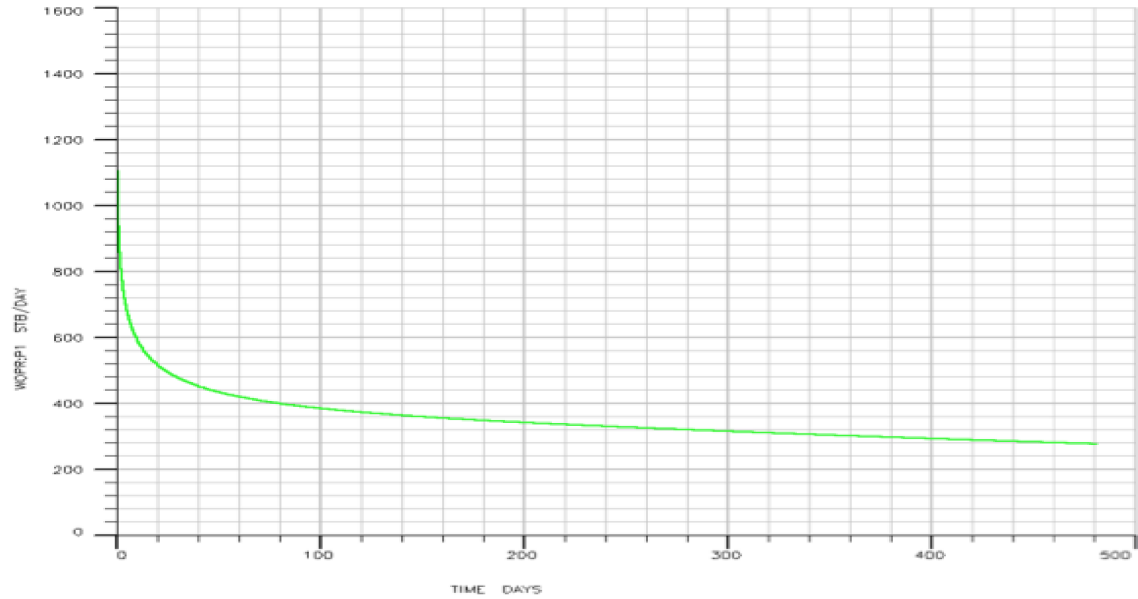
Figure 3.14: Oil production rate from a fracture treated with gelled acid.
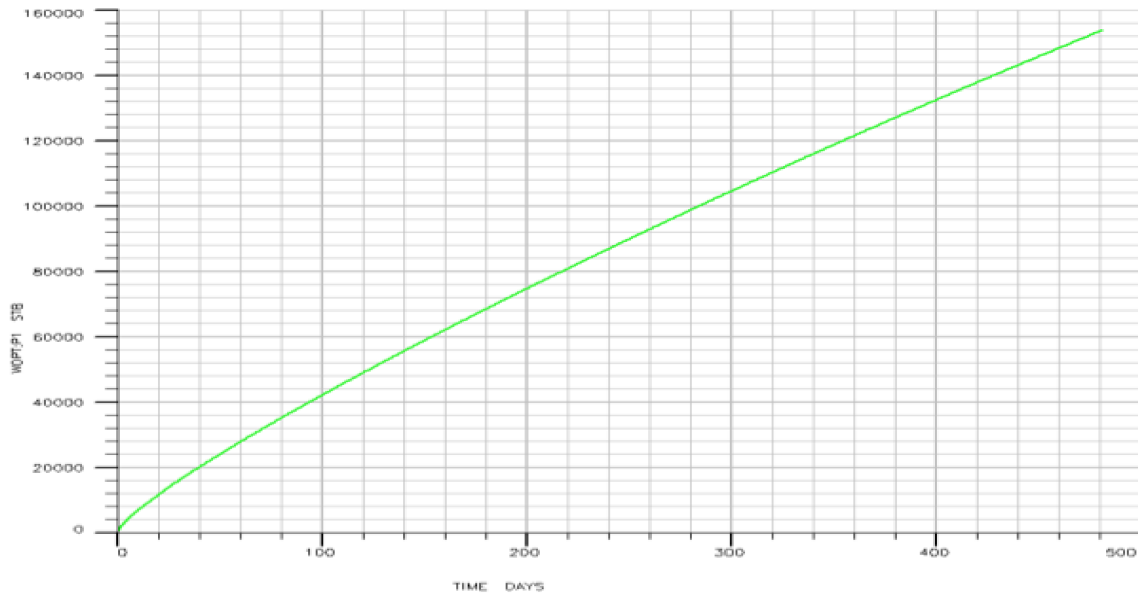
Figure 3.15: Cumulative oil production from a fracture treated with gelled acid

At a relatively high permeability (0.57 md), a gelled acid treatment results in the highest cumulative production rate and the closest to the optimum dimensionless fracture conductivity. Emulsified acid on the other hand, results in the lowest cumulative production rate. As the permeability is reduced to approximately 0.1 md, the emulsified acid outperforms straight acid in terms of production but the gelled acid is still the optimum choice. Dimensionless fracture conductivity (C_{fD}) did not show a relation with the cumulative production rate at lower permeability. When the reservoir permeability reaches roughly 0.01 md, emulsified acid becomes the optimum choice while straight acid is the least favorable one. The accumulative production is summarized in Table 3.4 and plotted in Figure 3.16.

Table 3.4: Oil cumulative production and dimensionless fracture conductivity for the ECLIPSE reservoir simulator cases.

Acid type	xf	Avg. $k_f.w$ (md.ft)	k=.57 md		k= .1 md		k= .05 md		k= .01 md	
			Q (STB)	CfD	Q (STB)	CfD	Q (STB)	CfD	Q (STB)	CfD
Straight	120	185	153000	2.70	44000	15.42	27000	30.83	8600	154.17
Gelled	240	170	168000	1.24	58000	7.08	38000	14.17	13400	70.83
Emulsified	320	37	112000	0.20	45000	1.16	33000	2.31	15400	11.56
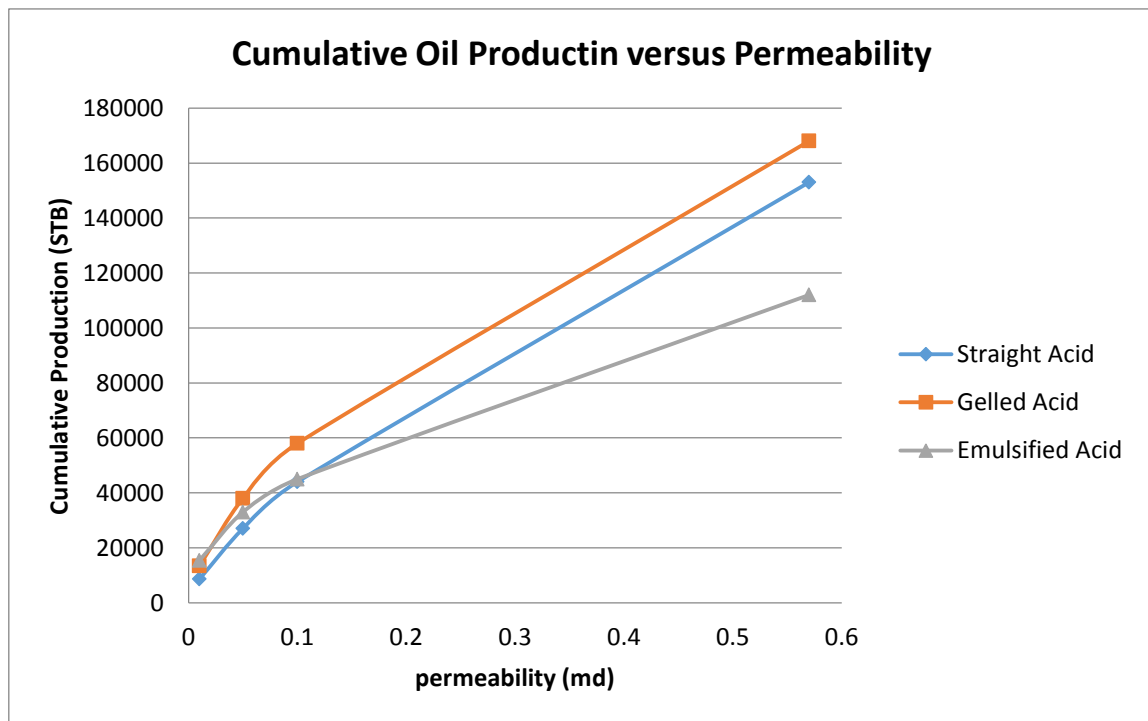
Figure 3.16: The cumulative oil production as function of reservoir permeability for the three acid systems.

It can be concluded that at relatively high permeability formations, creating short and highly conductive fracture is better option than creating long and low conductivity one. Hence, gelled acid and sometimes straight acid should be the optimum choices since they have great etching potential but can't reach very long distances in the fracture. As the formation becomes tighter, the fracture will mostly act like an infinite conductive fracture, even at low-conductivity values. This conclusion is based on the dimensionless fracture conductivity values (C_{fD}) that are higher than 100 for the three acid systems with roughly 0.01 md permeabilities. In this case, maximizing the acid-penetration distance is the key factor for higher production rates that can be achieved by using an emulsified acid or any high-viscosity fluid. In fact, increased etching volume does not add to a production improvement in this case. This conclusion is supported by field data from more than 70 wells in the Khuff formation within the Saudi Arabia Ghawar field. Straight acid, emulsified acid, and in-situ gelled acid are used where emulsified acid proved to be more suitable in low-permeability zones (Bartko et al., 2003)

3.2 Multistage Acid Injection

Acid fracturing consists of many steps where acid and pad fluids are injected in a stage- wise procedure. The assumption of the model is that pad fluid will be injected first and that will determine fracture height, length, and width. Then, acid is injected to etch the wall of the fracture without changing fracture geometry. Multiple fluid systems are used in field operations to obtain the benefit of each fluid system. Gelled acid could be injected together with emulsified acid or crosslinked acid to achieve additional etching

53

and greater penetration distances. The simulator has the option to run more than one acid

system. In this case, an emulsified acid is injected for 20 minutes to reach the tip of

fracture followed by gelled acid for roughly 10 minutes to increase the fracture

conductivity. The result of this treatment is better than treating a fracture with 30

minutes of emulsified acid alone (Fig. 3.17). Many combinations of acid systems can be

simulated to achieve an optimum fracture conductivity and penetration distance.
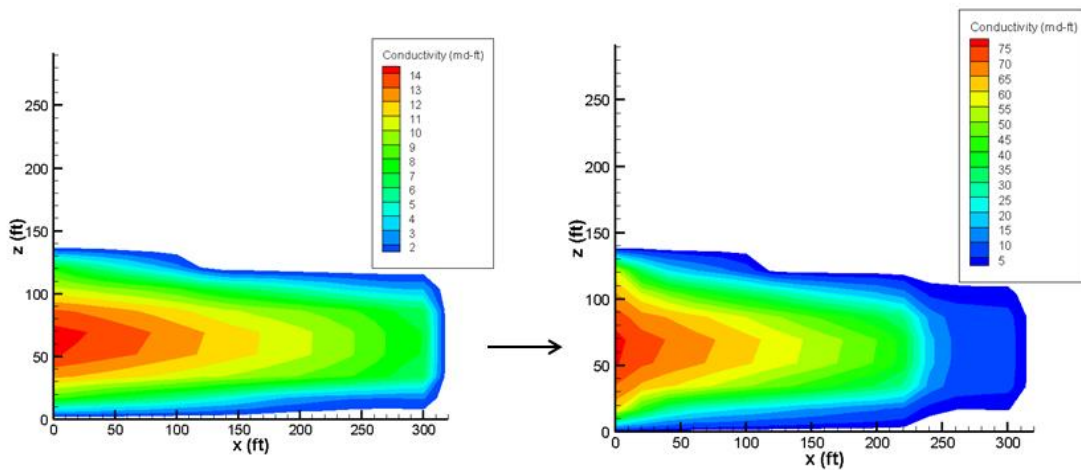
Figure 3.17: Conductivity profile for emulsified acid in the left and conductivity profile for gelled acid used as second stage in the right.

3.3 Diffusion Coefficient

Because the reaction rate is so fast, the diffusion step is the controlling step for

the reaction between HCl and the carbonate minerals. Modeling the acid diffusion lacks

diffusion coefficient data of acid systems as function of fracture width, roughness, fluid

loss rate, and Reynolds number. Therefore, the diffusion coefficient is assumed to be a

function of the fluid system and temperature only. This assumption causes diffusion modeling to be inaccurate and an imprecise representative of fluid diffusion behavior in field conditions. At a high-Peclet number, acid fracturing is fluid loss control, which means acid spending through diffusion will have no impact on the penetration distance. All of the cases run in the simulator have high-Peclet numbers (1 and above); hence, the expectation is that when the diffusion coefficient is changed, penetration distance will not be affected.

Straight acid is simulated in this case with different diffusion coefficients to demonstrate that the fluid-loss limit will dominate the result of the treatment in this case. All input parameters are held constant except for the diffusion coefficient. Figure 3.18 shows that penetration distance for straight acid is approximately 110 ft regardless of the diffusion coefficient value. In terms of conductivity, a higher diffusion coefficient leads to higher etching potential, which results in higher conductivity based on the Mou-Deng correlation. When the Peclet number falls below 1.0, acid spending through diffusion will control the penetration distance; however, the simulator fails to capture this phenomena because the simulator terminates at very high diffusion values.
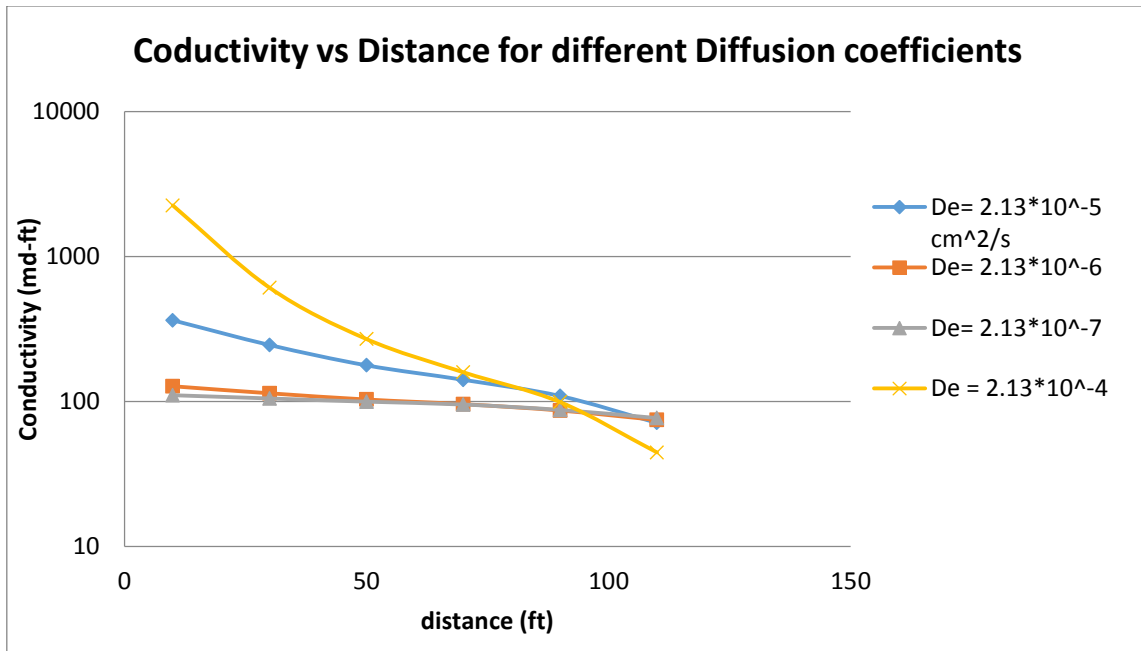
Figure 3.18: Conductivity along fracture length for different diffusion coefficient of straight acid.

3.4 Injection Rate and Formation Type

Because the injection rate has to be equal to the leakoff rate, and because the leakoff velocity does not change with injection rate, the leakoff distance will increase with an increase in injection rate. The correlation between injection rate and penetration distance is almost linear as shown in Figure 3.19. Increasing the injection rate will increase the amount of acid reacting with the fracture walls, which results in additional etched volume and high conductivity according to the Mou-Deng correlation. Formation type also has an impact on the penetration distance. A dolomite formation is far less reactive than a calcite formation; therefore, an increase in pore volume to break through

the formation is needed for dolomite ($Q_{ibt} = 20$) than for calcite ($Q_{ibt} = 1.5$). This result

means that a dolomite formation will have a lower leakoff coefficient and therefore, acid

will be able to travel a longer distance in the fracture. This conclusion is also shown in

Figure 3.19 where a dolomite formation results in a higher penetration distance at any

injection rate. In terms of conductivity, the calcite fracture shows higher conductivity

when compared with a dolomite fracture according to Mou-Deng correlations (Fig.

3.20).
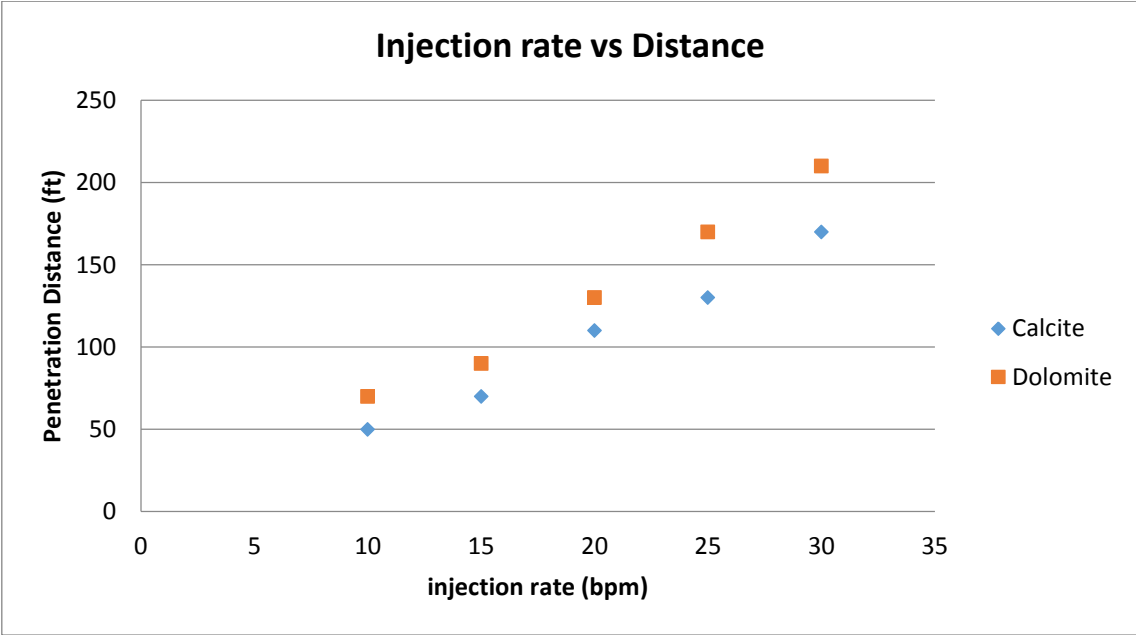
Figure 3.19: Injection rate versus penetration distance for a calcite and dolomite formations.
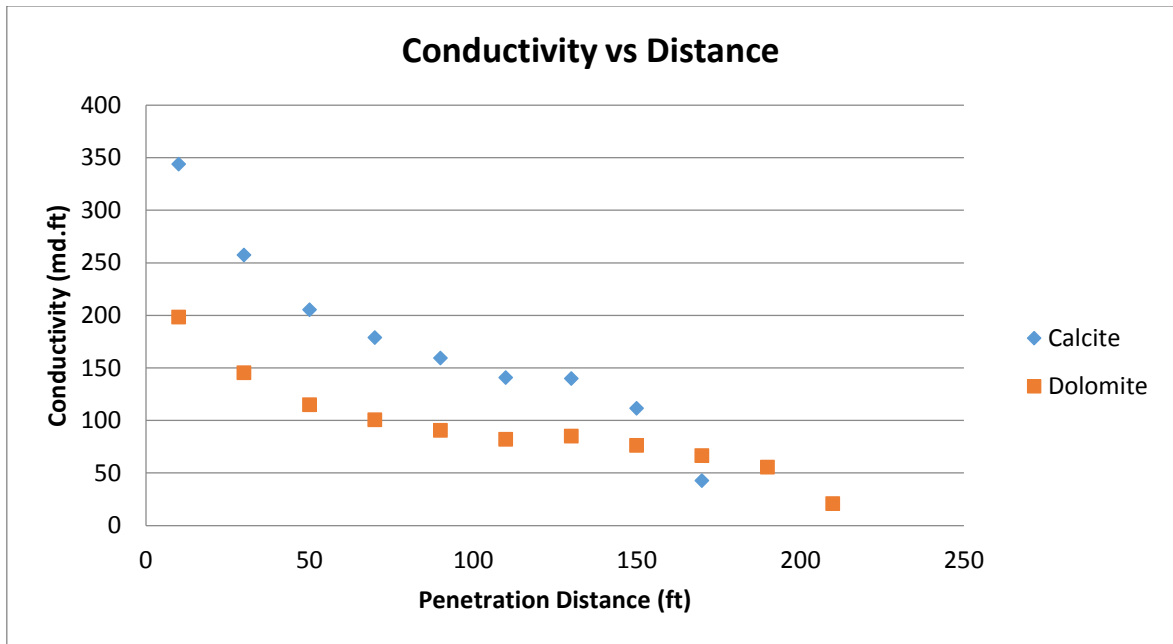
Figure 3.20: Conductivity versus distance for a calcite and dolomite formations.

3.5 Fracture Width

In a reaction-rate limit case, the fracture width has an impact on the penetration

distance where a wider fracture results in a greater acid-penetration distance. However,

the fracture width has no impact on penetration distance in a fluid-loss limit case. A

simple fracture shape that has a constant width is used to simulate different values of

fracture widths. Gelled acid is the fluid system used to simulate this case. Figure 3.21

shows fracture width values ranging from 0.05 in. to 0.3 in. where fracture conductivity

reaches zero at approximately 240 ft for all cases. A low-fracture width results in higher

etching potential and higher conductivity because a lower fracture width has a higher

acid gradient, which is the driving force for acid diffusion. This effect is more noticeable

at the fracture entrance and diminishes as the acid travels deeper into the fracture. It is necessary to mention that the conductivity is function of the acid etched width which is different from the width created because of the hydraulic effect.
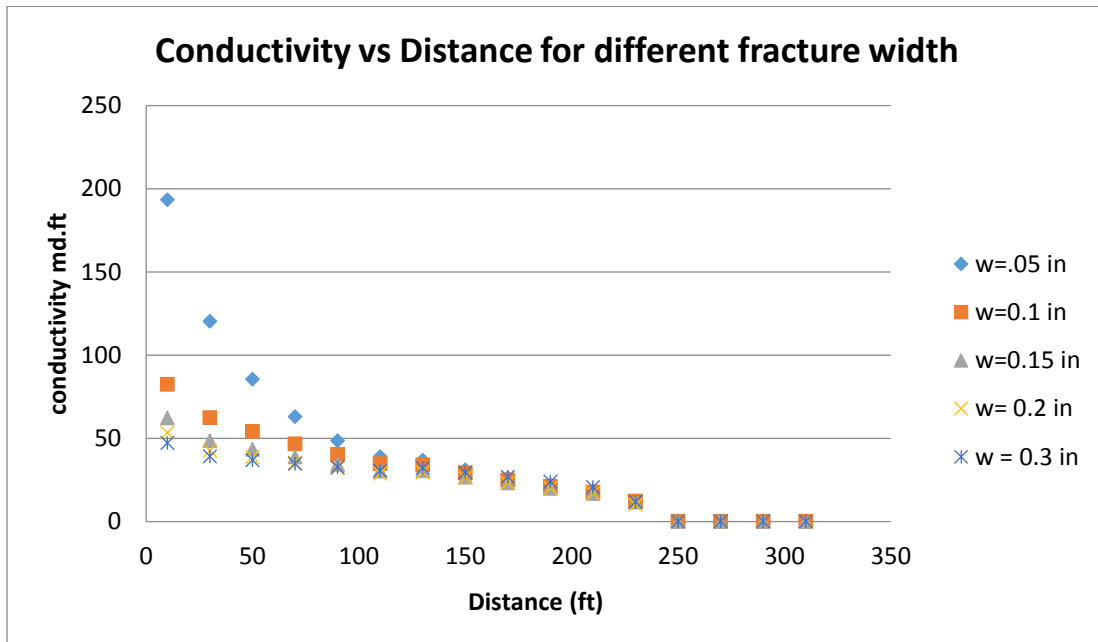
Figure 3.21: Conductivity versus distance for different values of fracture width.

3.6 Formation Permeability and Porosity

Both the effluent viscosity coefficient (Cv) and the reservoir fluid viscosity coefficient (Cc) are linearly increasing with the square root of reservoir permeability. Therefore, highly permeable formations result in a low-penetration distance because of the excessive leakoff rate. This relation is shown clearly in Figure 3.22 where the

penetration distance is increasing greatly as the reservoir permeability becomes tighter. Because the permeable formations result in a high leakoff rate, additional acid will react with the formation walls, resulting in additional etching when compared with tight formations. Figure 3.23 shows a comparison case between 2.0-md and 0.1-md formations where treating the higher permeable formation results in several orders of magnitude higher conductivity values. However, the conductivity will soon diminish to zero because the acid could not penetrate deeper inside of the fracture. Porosity has exactly the same effect on permeability in terms of conductivity and fracture penetration distance.

Permeability vs Distance
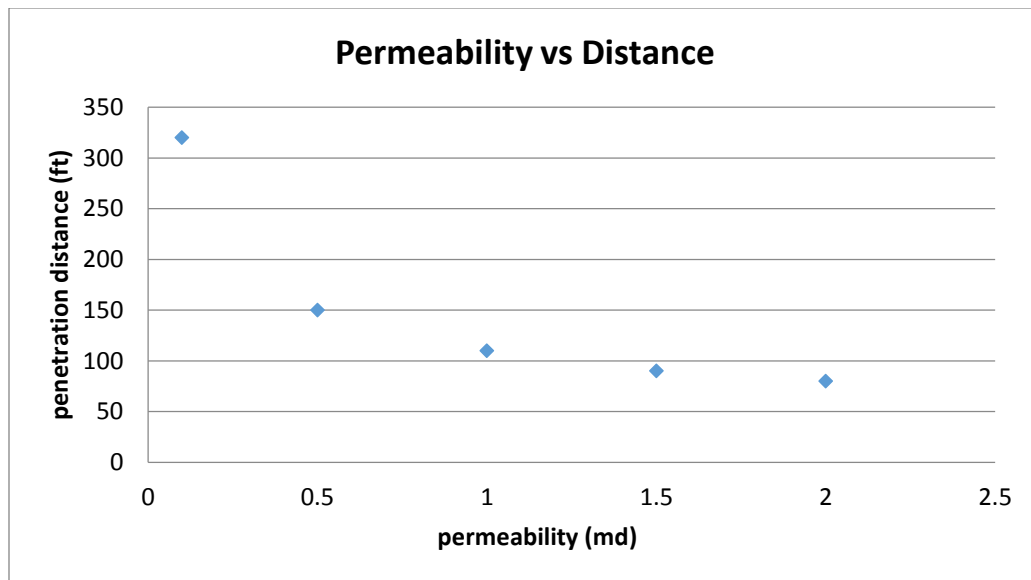
Figure 3.22: Penetration distance for different reservoir permeability values.
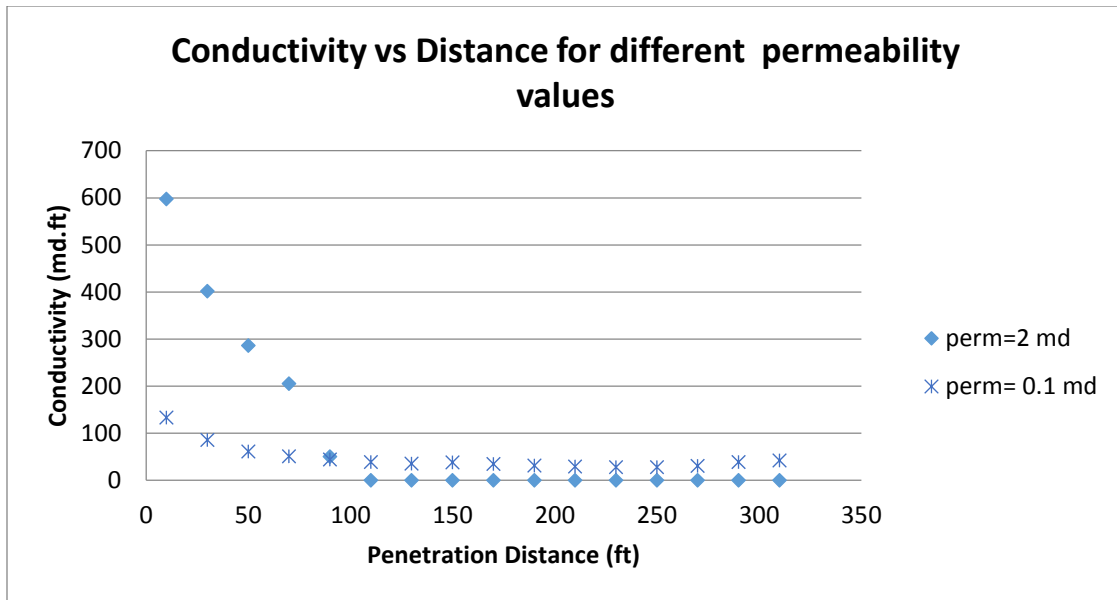
Figure 3.23: Conductivity versus distance for different reservoir permeability values.

3.7 Perforation Interval

The user has the option to select the length of the perforation interval for acid injection. Perforation has no impact on etching or the conductivity profile shape except at the fracture entrance as shown in Figure 3.24. Decreasing the perforation interval has a marginal benefit in terms of the conductivity value, which results in a 10% increase in the conductive fracture for the best cases. However, changing the perforation interval will have no impact on the penetration distance as shown in Figure 3.25. The simulator allows for selecting many perforation intervals along with fracture height.
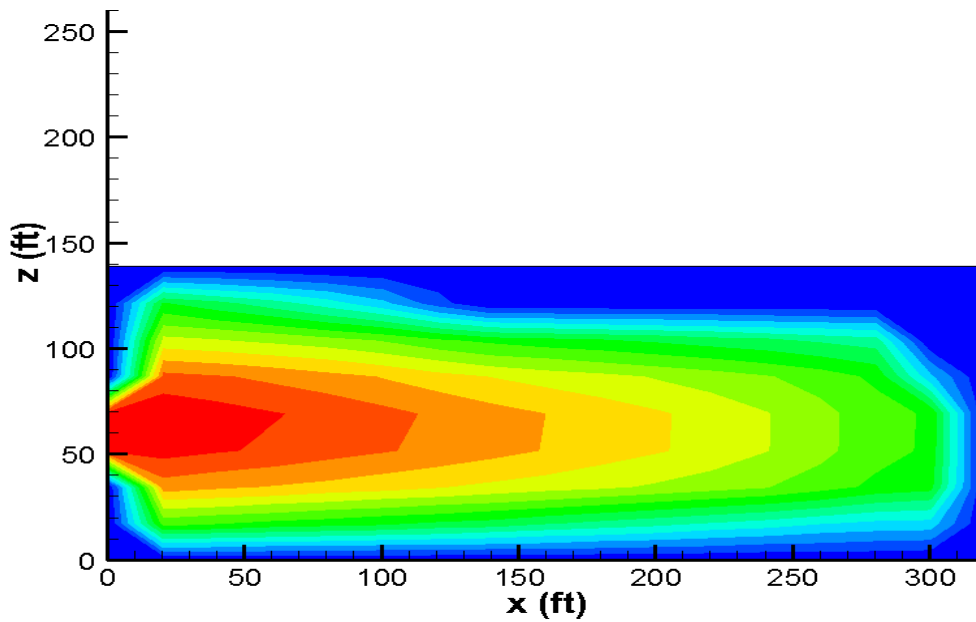
Figure3.24: Conductivity profile for emulsified acid that has 40 ft perforation interval at the fracture entrance.
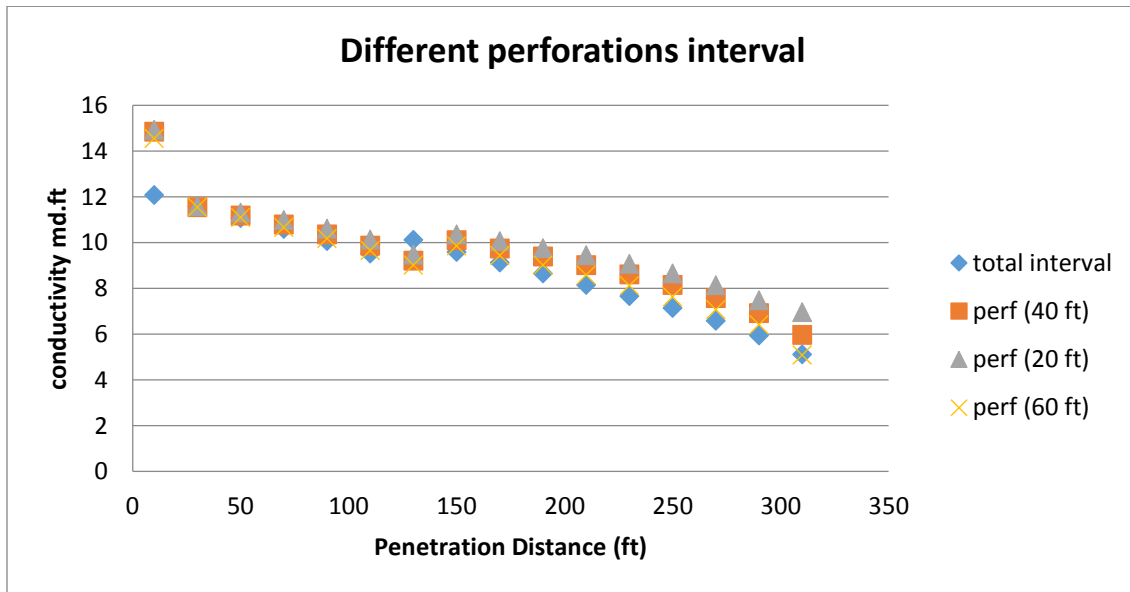
Figure 3.25: Conductivity vs distance for different perforation intervals.

CHAPTER IV

MODEL LIMITATIONS

4.1 Limitations Due to Model Assumptions

To solve the governing equations in this model, many assumptions are considered (discussed in Chapter 2). These assumptions can be a source of imprecision, but in such a stochastic process, these errors can be negligible when compared with errors caused by formation heterogeneity. The ability to quantify the amount of inaccuracy due to these assumptions will enable us to validate or reject these assumptions.

When acid reacts with the fracture wall, the heat from the reaction is released and transferred by convection due to fluid movement and conduction through the fracture walls. Temperature will continuously change during acid injection because this phenomenon has an impact on the rate of acid reaction and the amount of rock dissolved. To account for these effects, energy balance equations and the heat transfer equation should be considered, both of which will add complexity to the model. This model does not account for heat transfer and assumes an isothermal temperature.

Gravity has an impact on the fluid flow behavior that may add complexity to the flow in the fracture height direction. Also, gravity will allow the fluid to concentrate more in the bottom of the fracture. This condition will affect the acid etching profile; hence, the conductivity profile inside of the fracture. Many fracturing models do not

account for gravity and assume that it has negligible effect. This model excludes gravity, assuming the effect will be insignificant.

The model can simulate multistage processes of different acid systems but does not couple it with the mechanical behavior of the fracture. All pad fluid is assumed to be pumped as one stage to create a fixed fracture geometry that will not change during acid injection. Fracture geometry is imported from other commercial simulators; however, only acid injection will be simulated in our simulator. In field cases, acid and pad fluids are injected in a stage-wise process, which means acid injection will impact fracture geometry. Failure to couple acid injection with the geometry model can result in significant error and is considered the major limitation of the model. In the coupled case, fracture length, width, and height will keep changing during most of the stages.

The reservoir is assumed to be layered, which means the simulator will allow for entering properties of each layer instead of properties of each grid block; thus, the user has to specify each layer permeability and mineralogy. This procedure is valid for short fractures, but could be an invalid assumption for very long fractures.

4.2 Limitations Due to Numerical Errors

The SIMPLE algorithm is used to solve the Navier- Stokes equations. The consistency index (k) and the power low exponent (n) values have a large impact on the solution stability of the simulator. Some values will result in numerical errors that cause the simulator to terminate without completing the run. Pressure inside of the fracture should be maintained at an almost constant value during injection time; however, an unstable solution makes the pressure drop quickly at each time step until the pressure reaches zero, and hence, the simulation terminates. A high-diffusion coefficient also can cause a decrease of pressure inside of the fracture to zero, which imposes an upper limit on the diffusion coefficient value. Changing the number of grid blocks or the size of each grid block causes the solution to terminate if not changed proportionally. These numerical errors place a limit on the various simulation cases that can be run in this simulator.

For the PKN geometry model, the width of the fracture is assumed to decrease gradually until reaching the tip of the fracture. The geometry used in most of the cases shows a sharp decrease in fracture height at the middle of the fracture. As Figure 4.1 shows, conductivity suddenly increased at that location because the fluid has to converge to the smaller fracture opening.
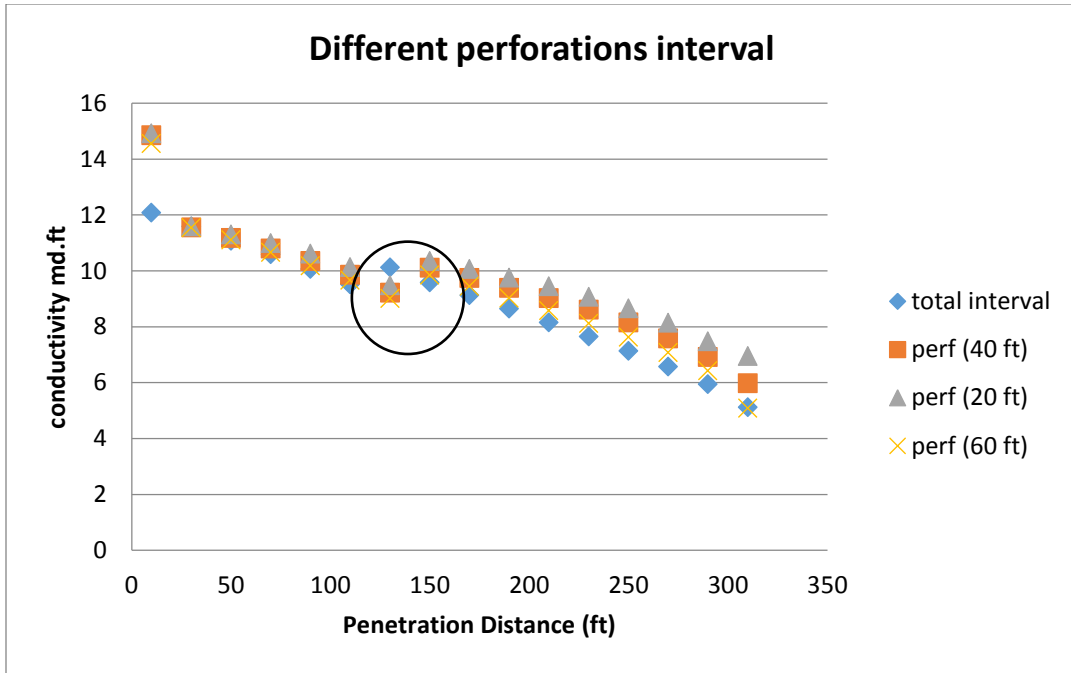
Figure 4.1: A sudden increase in conductivity value in the middle of the fracture.

This condition is not possible because the acid concentration must be decreasing with distance as well as the volume of acid due to leakoff into the fracture walls. One possible explanation of this error is that the value of the volumetric dissolving power constant was kept even though the concentration of acid reacting with fracture wall must be decreasing. The amount of conductivity increase in this case is negligible and the conductivity profile continues to decrease after this point.

For acid with a high-diffusion coefficient such as straight acid and gelled acid, excessive fracture conductivity appears at the top and bottom of the fracture entrance. This effect is not shown when acid has very low-diffusion coefficient as with emulsified acid. One possible explanation of this behavior is that the acid gradient is higher at smaller widths, which results in higher acid diffusion through the fracture wall; however,

this condition will result in additional etching at the fracture edges, which is not physical. Further investigation of this behavior showed that the acid diffusion is very large because of the assumption that acid concentration at the fracture entrance is the initial concentration while acid concentration at the fracture walls is almost zero. Thus, excessive etching will occur and high-conductivity contours will be shown at the top and bottom of the fracture entrance. Finer gridding at the fracture entrance will limit the initial concentration range to only 1 ft or less instead of 20 ft from the fracture entrance and may result in a more homogenous concentration profile.
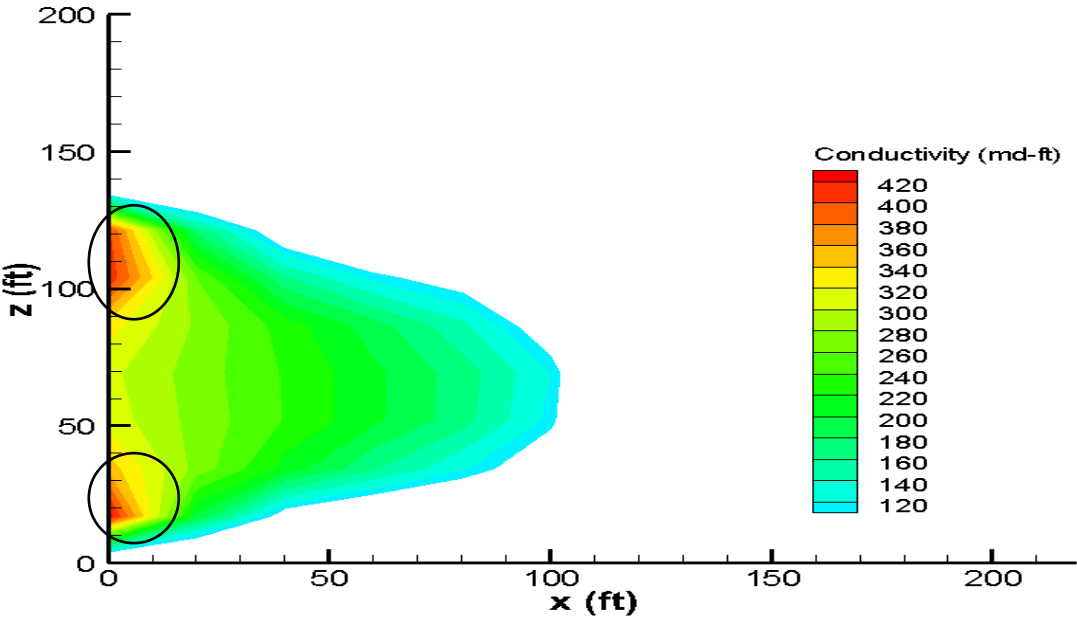
Figure 4.2: Excessive fracture conductivity at upper and lower points at the fracture entrance

CHAPTER V

CONCLUSION AND RECOMMENDATIONS

5.1 Conclusion

Acid fracturing is a well stimulation technique used in carbonate reservoirs.

Developing a theortical model can help to optimize the treatment parameters for acid

fracturing. The model developed uses other commercial software to import the initial

fracture geometry. The Navier-Stokes (momentum balance) and continuity (mass

balance) equations are solved for pressure and velocity profiles. Once the velocity

profile is computed, the acid balance equation can be solved for the acid concentration

profile. Obtaining a concentration profile helps in calculating the amount of rock etched

through diffusion and convection (leaking through fracture walls). Conductivity

distribution is calculated using the Deng-Mou correlation where statistical parameters

are used to account for fracture heterogeneity. This conductivity distribution can be

imported to other reservoir simulators such as the ECLIPSE simulator to compute the

production rate after completing the treatment.

Two important parameters will determine a production increase from a fractured

well; these are fracture conductivity and acid penetration distance. Straight acid, gelled

acid, and emulsified acid are simulated to observe the effect of these fluids on the two

parameters. Straight acid shows strong etching potential, resulting in high conductivity

but it leaks off completely near the fracture entrance. Gelled acid has a medium etching

strength and can reach greater distances than with straight acid. Emulsified acid has the

lowest etching potential, resulting in the lowest conductivity but it reaches greater distances than the other acid systems. Conductivity distributions along the fracture are imported into the ECLIPSE Simulator to simulate production rates for each case. In high-permeability formations, gelled acid results in the highest production rate because high conductivity is more favorable than low conductivity and a long penetration distance. In low-permeability formations, emulsified acid yields the best results because the acid penetration distance is more favorable in this case than creating short and high-conductivity fractures. A combination of the different acid systems can result in the optimum production case where the simulator allows for using more than one stage of an acid system.

The fluid loss limit case is assumed in this simulator, which means nothing will alter the acid penetration distance except for the parameters that affect the leakoff coefficient. Hence, the diffusion coefficient will have no impact on the acid penetration distance but it will affect the fracture conductivity value. A higher injection rate will result in a greater penetration distance and increased conductivity because a higher volume of acid is pumped. Acid tends to travel a greater distance in fractures in dolomite than in calcite. The reason for this result is that dolomite is far more resistible to wormholing than is calcite. Nevertheless, acid will create more etching in calcite, resulting in better conductivity when assuming the Deng-Mou correlation. The fracture width impacts the penetration distance in the reaction rate limit case where a wider fracture will allow fluid to travel a greater distance in the fracture. However, in the fluid loss limit case, the fracture width will not affect the acid penetration distance but it will

have an impact on the conductivity value where a lower width gives better conductivity. Formation permeability and porosity will have similar effects. A more porous and permeable formation usually results in a lower penetration distance because of higher leakoff rate. On the other hand, more etching will result from acid leaking through the fracture wall. A simulator allows the user to specify the perforation interval, where a smaller perforation range results in a marginal increase in the average conductivity value; however, changing the length of perforation interval will not have any impact on the penetration distance.

5.2 Recommendations

Coupling an acid fracturing model with a geomechanical model to simulate fracture propagation as fluid is injected should be considered. This model will allow for making more accurate fracture geometry predictions in terms of height, length, and width. Also, including a heat transfer model makes the fracture model more powerful because temperature has a strong impact on the reaction rate between an acid and carbonate minerals. Including a temperature profile makes the simulator more representatives of filed applications. However, before including heat transfer and geomechanical models, numerical errors resulting from Navier-Stokes equations should be solved to make the simulator more stable. Changing fracture geometry or other treatment parameters can result in a rapid decrease in pressure inside of the fracture,

which causes the simulator to stop early in the process. Solving this problem is the first

priority before coupling the model.

REFERENCES

Bartko, K.M., Nasr-El-Din, H.A., Rahim, Z., and Al-Muntasheri, G.A. 2003. Acid Fracturing of a Gas Carbonate Reservoir: The Impact of Acid Type and Lithology on Fracture Half Length and Width. Paper SPE 84130 presented at the SPE Annual Technical Conference and Exhibition, Denver, Colorado, 5-8 October.

Ben-Naceur, K. and Economides, M.J. 1989. Design and Evaluation of Acid Fracturing Treatments. Paper SPE 18978 presented at the SPE Joint Rocky Mountain Regional/Low Permeability Reservoirs Symposium and Exhibition, Denver, Colorado, 6-8 March.

Crowe, C.W., Martin, R.C., and Michaelis, A.M. 1981. Evaluation of Acid-Gelling Agents for Use in Well Stimulation. *SPEJ* **21**(2): 415-424.

De Rozieres, J. 1994. Measuring Diffusion Coefficients in Acid Fracturing Fluids and Their Application to Gelled and Emulsified Acids. Paper SPE 28552 presented at the SPE Annual Technical Conference and Exhibition, New Orleans, Louisiana, 25-28 September.

Deng, J., Mou, J., Hill, A.D., and Zhu, D. 2012. A New Correlation of Acid-Fracture Conductivity Subject to Closure Stress. *SPE Prod. & Oper.* **27**(2): 158-169.

Economides, M.J., Hill, A.D., and Ehlig-Economides, C. 1994. *Petroleum Production Systems*. Upper Saddle River, New Jersey: Prentice Hall, PTR.

Gdanski, R.D., and Lee, W.S. 1989. On the Design of Fracture Acidizing Treatments. Paper SPE 18885 presented at the SPE Production Operations Symposium, Oklahoma City, Oklahoma, 13-14 March.

Hill, A.D., Zhu, D., and Wang, Y. 1995. The Effect of Wormholing on the Fluid-Loss Coefficient in Acid Fracturing. *SPE Prod. Fac.* **10**(4): 257-263.

Kalfayan, L.J. 2007. Fracture Acidizing: History, Present State, and Future. Paper SPE 106371 presented at the SPE Hydraulic Fracturing Technology Conference, College Station, Texas, 29-31 January.

Lo, K.K. and Dean, R.H. 1989. Modeling of Acid Fracturing. *SPE Prod. Eng.* **4**(2): 194-200.

Mou, J. 2009. Modeling Acid Transport and Non-Uniform Etching in a Stochastic Domain in Acid Fracturing. Ph.D. dissertation, College Station: Texas A&M University.

Mou, J., Zhu, D., and Hill, A.D. 2010. Acid-Etched Channels in Heterogeneous Carbonates–A Newly Discovered Mechanism for Creating Acid-Fracture Conductivity. *SPEJ* **15**(2): 404-416.

Nierode, D.E., Williams, B.R., and Bombardieri, C.C. 1972. Prediction of Stimulation from Acid Fracturing Treatments. *JCPT* **11**(4): 31-41

Nierode, D.E. and Kruk, K.F. 1973. An Evaluation of Acid Fluid Loss Additives, Retarded Acids, and Acidized Fracture Conductivity. Paper SPE 4549 presented at the SPE Annual Fall Meeting, Las Vegas, Nevada, 30 September – 3 October.

Nierode, D.E. and Williams, B.B. 1971. Characteristics of Acid Reaction in Limestone Formations. *SPEJ* **11**(4): 406-418.

Nieto, C.M., Pournik, M., and Hill, A.D. 2008. The Texture of Acidized Fracture Surfaces: Implications for Acid Fracture Conductivity. *SPE Prod. & Oper.* **23**(3): 343-352.

Oeth, C. 2013. Three Dimensional Modeling of Acid Transport and Etching in a Fracture. Ph.D. dissertation, College Station: Texas A&M University.

Oeth, C.V., Hill, A.D., and Zhu, D. 2014. Acid Fracture Treatment Design with Three-Dimensional Simulation. Paper SPE 168602 presented at the SPE Hydraulic Fracturing Technology Conference, The Woodlands, Texas, 4-6 February.

Penny, G.S. and Conway, M.W. 1989. Chapter 8, Fluid Leakoff. In *Recent Advances in Hydraulic Fracturing*, eds. J.L. Gidley, S.A. Holditch, D.E. Nierode, and R.W. Veatch, Jr., 388-393. Richardson, Texas: Society of Petroleum Engineers.

Schechter, Robert S. 1992. *Oil Well Stimulation*. Englewood Cliffs, New Jersey: Prentice-Hall, Inc.

Settari, A. 1993. Modeling of Acid-Fracturing Treatments. *SPE Prod. & Fac.* **8**(1): 30-38.
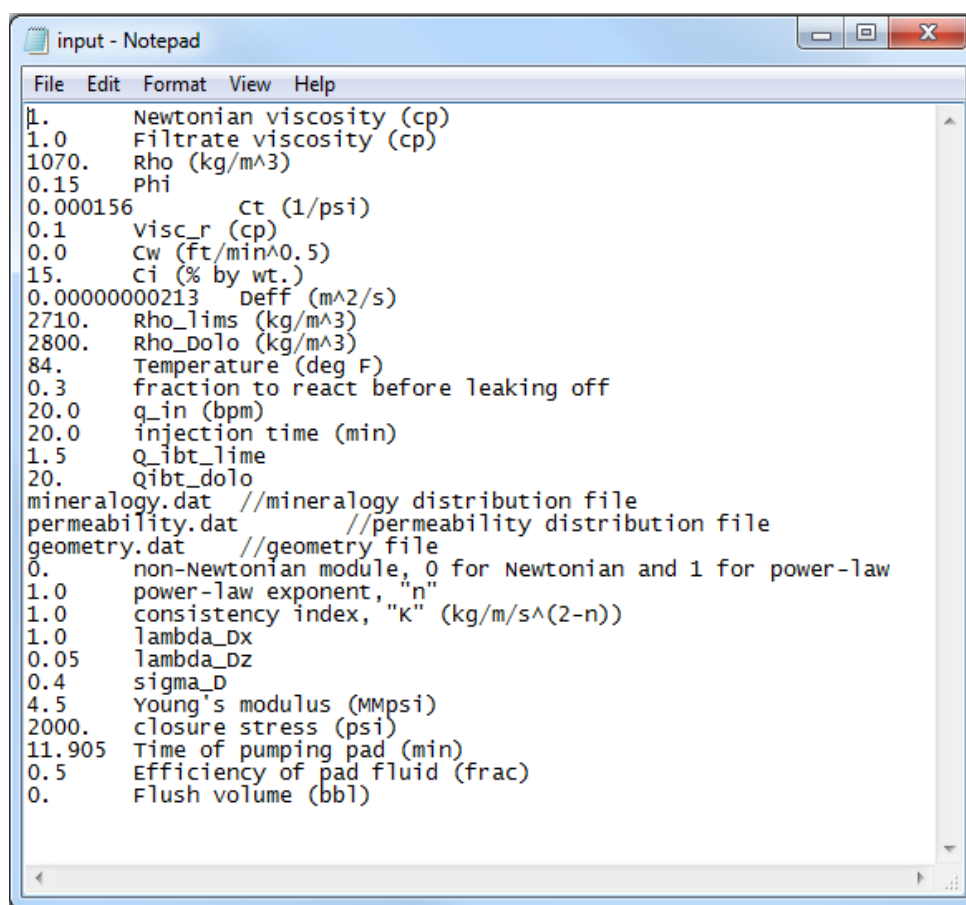
Settari, A., Sullivan, R.B., and Hansen, C. 2001. A New Two-Dimensional Model for Acid-Fracturing Design. *SPE Prod. & Fac.* **16**(4): 200-209.

Williams, B.B. and Nierode, D.E. 1972. Design of Acid Fracturing Treatments. *JPT* **24**(7): 849-859.

Williams, B.B., Gidley, J.L., and Schechter, R.S. 1979. *Acidizing Fundamentals*. Dallas, Texas: Society of Petroleum Engineers of AIME.

Appendix A shows the four input files for acid fracturing simulator. These are the only files for user to input data to run the simulator. These files are; main input file, geometry shape file, permeability distribution file, and mineralogy distribution file.

Figure A.1: Main input file for the acid fracturing simulator.
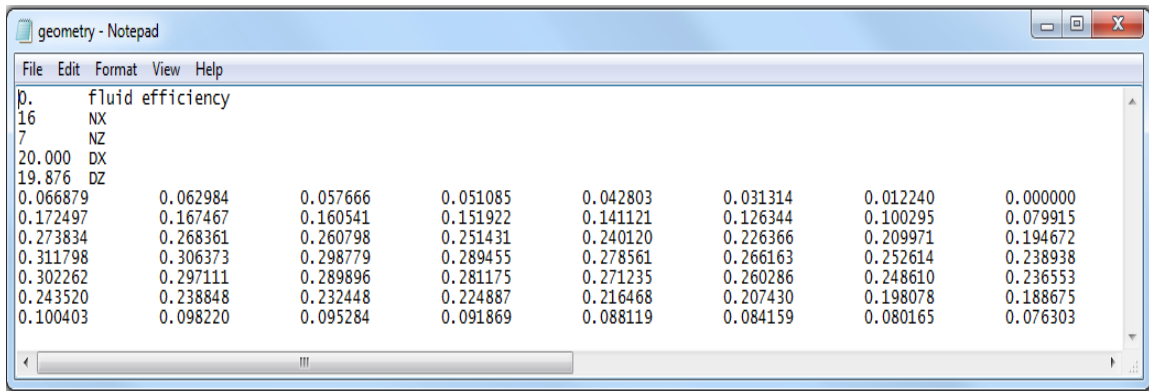
Figure A.2: Geometry imported to the acid fracturing simulator.
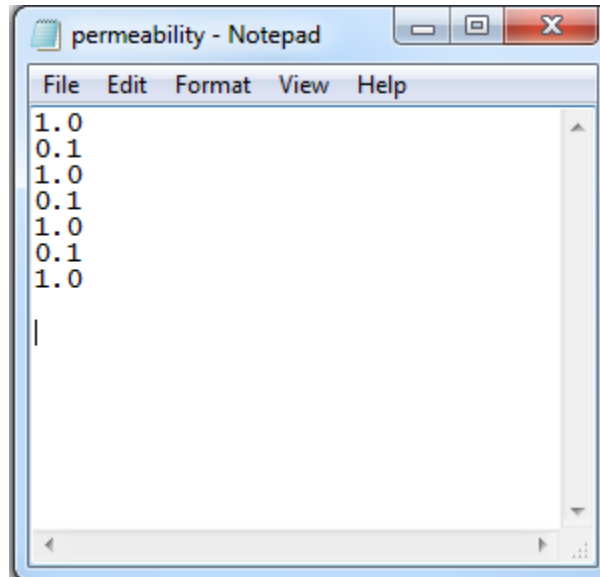
Figure A.3: Permeability distribution in the fracture, one value per layer.
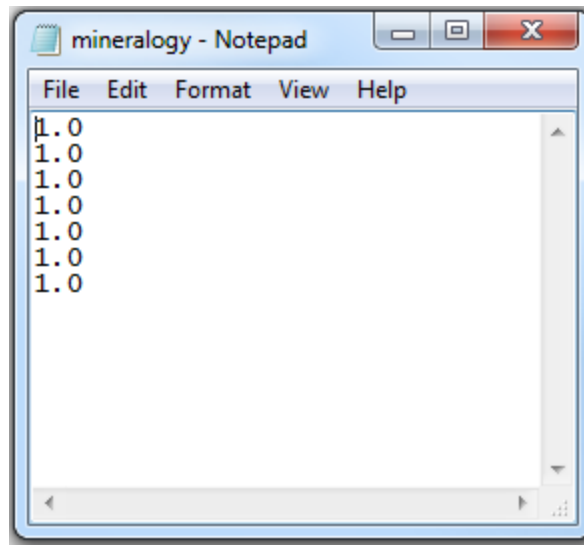
Figure A.4: Mineralogy distribution in the fracture, one value per layer where 1.0 refers to calcite, 0 refers to dolomite.

APPENDIX B

Appendix B shows the three input files for the ECLIPSE reservoir simulator. The main input file is to create the reservoir and fluid properties and to specify the gridding pattern for the reservoir. The well specification file is used to specify the perforation interval for production, well location and the production mode of the well (constant rate or constant pressure). The permeability distribution file is used to specify the permeability of the reservoir and the fracture after converting conductivity into permeability assuming constant fracture width of 0.1 inch.

```
RUNSPEC

DIMENS
93 21 25
/


FIELD

OIL

WATER

START
1 MAR 2012
/

WELLDIMS
1 126 1 1
/

TABDIMS
    1    1   25   12    1   12 /

GRID

GRIDFILE
2
/

INIT

DXV
3*25 27*20 16*20 1*0.1 16*20 27*20 3*25
/

DYV
5*100 1*92.5 1*90 1*50 1*30 1*15.5 1*0.1 1*15.5 1*30 1*50 1*90 1*92.5 5*100
/

BOX
        1 93 1 21 1 1 /
TOPS
1953*6805 /
ENDBOX

DZ
1953*5
1953*5
1953*5
1953*5
1953*5
1953*5
1953*5
1953*5
1953*5
1953*19.876
1953*19.876
1953*19.876
1953*19.876
1953*19.876
1953*19.876
1953*19.876
1953*5
1953*5
1953*5
1953*5
1953*5
1953*5
```

```
PORO
48825*0.15 /

INCLUDE
FS_PERM.DATA_GRI   /

COPY
        PERMX   PERMY /
        PERMX   PERMZ /
/

PROPS

PVDO
            1000            1.259           1.1500
            1200            1.241           1.1300
            3400            1.239           0.9500 /

PVTW
4015      1.046506991       2.5118E-06        0.324362224       5.38605E-05 /



DENSITY
41.9     65.25339878      0.087917234 /


SWOF
--     Sw              Krw             Krnw            PC
--(frac PV)                                           (psi)

   0.0000          0.0000          1.0000          1*
   0.0145          0.0021          0.6409          1*
   0.0293          0.0148          0.4111          1*
   0.0504          0.0434          0.2604          1*
   0.0829          0.0995          0.1472          1*
   0.1223          0.1880          0.0741          1*
   0.1746          0.2923          0.0362          1*
   0.2777          0.4203          0.0150          1*
   0.3612          0.4746          0.0101          1*
   0.4400          0.5185          0.0072          1*
   0.5424          0.5739          0.0046          1*
   0.6083          0.6083          0.0034          1*
   0.6725          0.6414          0.0025          1*
   0.7356          0.6758          0.0017          1*
   0.7923          0.7072          0.0012          1* |
   0.8153          0.7232          0.0010          1*
   0.8774          0.7947          0.0004          1*
   0.9042          0.8644          0.0001          1*
   0.9244          0.9296          0.0000          1*
   0.9483          1.0000          0.0000          1* /


ROCK
6000 3.0E-5 /

REGIONS

SOLUTION

EQUIL
-- DEPTH | PRESSURE | OWC | Pc at OWC
6505 2900 9000 0   /

SUMMARY

RUNSUM
EXCEL
```

```
RUNSUM
EXCEL
WPI
/
WOPR
/
WOPRH
/
WOPT
/
WOPTH
/
WWPR
/
WWPRH
/
WWPT
/
WWPTH
/
WWIR
/
WWIRH
/
WWIT
/
WBHP
/
WBHPH
/


SCHEDULE

TUNING
--   TSINIT   TSMAXZ   TSMINZ   TSMCHP   TSFMAX   TSFMIN   TSFCNV   TFDIFF   THRUPT   TMAXWC
--      1.0    365.0      0.1     0.15               3.0      0.3      0.1     1.25    1E20         1* / -- Default
        1.0      1.0   1.E-10      1.0      3.0      0.3      0.1     1.25    1E20         1* /
--   TRGTTE   TRGCNV   TRGMBE   TRGLCV   XXXTTE   XXXCNV   XXXMBE   XXXLCV   XXXWFL   TRGFIP   TRGSFT
--      0.1    0.001   1.0E-7   1.0E-4     10.0   1.0E-2   1.0E-6   1.0E-3   1.0E-3    0.025         1* / -- Default
      0.001   0.0001   1.0E-9   0.0001     10.0   1.0E-5   1.0E-9    0.001    0.001    0.025         1* /
---  NEWTMX   NEWTMN   LITMAX   LITMIN   MXWSIT   MXWPIT   DDPLIM   DDSLIM   TRGDPR   XXXDPR
--      12        1       25        1        8        8    1.0E6    1.0E6    1.0E6    1.0E6  / -- Default
      5000        1     5000        1     1000      100     1000     1000     1000     1000  /
/

RPTRST
RESTART=2 ALLPROPS PRES /

INCLUDE
FS_Single.DATA_SCH /


END
```

Figure B.1: Main input file for the ECLIPSE reservoir simulator.

```
WELSPECS
 -- Well Name | Group |  I  |  J  | Ref Dep
        P1         A     47    11     1*      LIQ  3* 1* 3* /
/

COMPDAT
-- Well Name | I-loc | J-locn | K-Loc | K-loc | OPEN/OPEN | 1* | 1* | Well Diameter | Kh | Skin | 1* | Direction |
        P1       47      11       1       1       SHUT      1*   1*      0.73        1*    0     1*      X        /
        P1       47      11       2       2       SHUT      1*   1*      0.73        1*    0     1*      X        /
        P1       47      11       3       3       SHUT      1*   1*      0.73        1*    0     1*      X        /
        P1       47      11       4       4       SHUT      1*   1*      0.73        1*    0     1*      X        /
        P1       47      11       5       5       SHUT      1*   1*      0.73        1*    0     1*      X        /
        P1       47      11       6       6       SHUT      1*   1*      0.73        1*    0     1*      X        /
        P1       47      11       7       7       SHUT      1*   1*      0.73        1*    0     1*      X        /
        P1       47      11       8       8       SHUT      1*   1*      0.73        1*    0     1*      X        /
        P1       47      11       9       9       SHUT      1*   1*      0.73        1*    0     1*      X        /
        P1       47      11      10      10       OPEN      1*   1*      0.73        1*    0     1*      X        /
        P1       47      11      11      11       OPEN      1*   1*      0.73        1*    0     1*      X        /
        P1       47      11      12      12       OPEN      1*   1*      0.73        1*    0     1*      X        /
        P1       47      11      13      13       OPEN      1*   1*      0.73        1*    0     1*      X        /
        P1       47      11      14      14       OPEN      1*   1*      0.73        1*    0     1*      X        /
        P1       47      11      15      15       OPEN      1*   1*      0.73        1*    0     1*      X        /
        P1       47      11      16      16       OPEN      1*   1*      0.73        1*    0     1*      X        /
        P1       47      11      17      17       SHUT      1*   1*      0.73        1*    0     1*      X        /
        P1       47      11      18      18       SHUT      1*   1*      0.73        1*    0     1*      X        /
        P1       47      11      19      19       SHUT      1*   1*      0.73        1*    0     1*      X        /
        P1       47      11      20      20       SHUT      1*   1*      0.73        1*    0     1*      X        /
        P1       47      11      21      21       SHUT      1*   1*      0.73        1*    0     1*      X        /
        P1       47      11      22      22       SHUT      1*   1*      0.73        1*    0     1*      X        /
        P1       47      11      23      23       SHUT      1*   1*      0.73        1*    0     1*      X        /
        P1       47      11      24      24       SHUT      1*   1*      0.73        1*    0     1*      X        /
        P1       47      11      25      25       SHUT      1*   1*      0.73        1*    0     1*      X        /
/


WCONPROD
P1 OPEN BHP 1* 1* 1* 1* 1* 1500 1* 1* 1* 1* 1* 1* 1* 1* 1* 1* /
/

TSTEP
50*0.2
60*0.5
96*1
50*2
22*5
3*45 /
```

Figure B.2: Well specification file for the ECLIPSE reservoir simulator.

```
PERMX               --2                                  1*527.683474    1*442.194532    1*468.147658    30*0.57
1953*0.57           93*0.57          1*380.680687        1*1000000       1*452.068349    1*461.365401    93*0.57
1953*0.57           93*0.57          1*395.113125        1*527.683474    1*460.399317    1*454.6881      93*0.57
1953*0.57           93*0.57          1*406.584477        1*522.376395    1*468.965817    1*447.680753    93*0.57
1953*0.57           93*0.57          1*415.612848        1*515.591508    1*478.044668    1*440.564205    93*0.57
1953*0.57           93*0.57          1*423.511859        1*508.345134    1*486.212985    1*433.538345    93*0.57
1953*0.57           93*0.57          1*431.667862        1*500.027323    1*494.605977    1*427.121896    93*0.57
1953*0.57           93*0.57          1*439.609262        1*490.695342    1*502.34791     1*420.296837    93*0.57
1953*0.57           93*0.57          1*450.240985        1*480.501201    1*509.253577    1*412.079428    93*0.57
1953*0.57           93*0.57          1*462.198641        1*471.042647    1*515.858164    1*403.26558     93*0.57
--1                 30*0.57          1*471.713985        1*461.936063    1*521.068074    1*391.927965    93*0.57
93*0.57             1*179.514624     1*480.984267        1*452.693206    1*1000000       1*377.51783     93*0.57
93*0.57             1*180.646273     1*488.198845        1*442.720907    1*521.068074    1*358.708718    --8
93*0.57             1*190.777471     1*495.59473         1*431.279099    1*515.858164    1*345.829695    1953*0.57
93*0.57             1*208.803661     1*501.627851        1*418.207771    1*509.253577    30*0.57          1953*0.57
93*0.57             1*234.614541     1*1000000           1*400.830788    1*502.34791     93*0.57          1953*0.57
93*0.57             1*263.122586     1*501.627851        1*378.310423    1*494.605977    93*0.57          1953*0.57
93*0.57             1*294.045079     1*495.59473         1*364.001797    1*486.212985    93*0.57          1953*0.57
93*0.57             1*319.608839     1*488.198845        30*0.57         1*478.044668    93*0.57          1953*0.57
93*0.57             1*339.093436     1*480.984267        93*0.57         1*468.965817    93*0.57          1953*0.57
93*0.57             1*362.455213     1*471.713985        93*0.57         1*460.399317    93*0.57          1953*0.57
30*0.57             1*382.209767     1*462.198641        93*0.57         1*452.068349    93*0.57          1953*0.57
1*0.57              1*395.048674     1*450.240985        93*0.57         1*442.194532    93*0.57          1953*0.57
1*0.57              1*405.689997     1*439.609262        93*0.57         1*430.806528    93*0.57
1*0.57              1*414.835394     1*431.667862        93*0.57         1*417.784455    93*0.57
1*0.57              1*425.066531     1*423.511859        93*0.57         1*400.470641    93*0.57
1*0.57              1*434.28598      1*415.612848        93*0.57         1*377.877678    --7
1*0.57              1*1000000        1*406.584477        93*0.57         1*363.424355    93*0.57
1*0.57              1*434.28598      1*395.113125        93*0.57         30*0.57         93*0.57
1*0.57              1*425.066531     1*380.680687        --5             93*0.57         93*0.57
1*0.57              1*414.835394     1*362.15341         93*0.57         93*0.57         93*0.57
1*0.57              1*405.689997     1*349.633584        93*0.57         93*0.57         93*0.57
1*0.57              1*395.048674     30*0.57             93*0.57         93*0.57         93*0.57
1*155.626407        1*382.209767     93*0.57             93*0.57         93*0.57         93*0.57
1*216.267893        1*362.455213     93*0.57             93*0.57         93*0.57         93*0.57
1*265.795905        1*339.093436     93*0.57             93*0.57         93*0.57         93*0.57
1*315.858763        1*319.608839     93*0.57             93*0.57         93*0.57         30*0.57
1*374.060332        1*294.045079     93*0.57             93*0.57         93*0.57         1*113.560104
1*1000000           1*263.122586     93*0.57             93*0.57         93*0.57         1*103.985618
1*374.060332        1*234.614541     93*0.57             93*0.57         --6             1*100.030006
1*315.858763        1*208.803661     93*0.57             30*0.57         93*0.57         1*100.288517
1*265.795905        1*190.777471     93*0.57             1*363.424355    93*0.57         1*106.33594
1*216.267893        1*180.646273     --4                 1*377.877678    93*0.57         1*119.937604
1*155.626407        1*179.514624     93*0.57             1*400.470641    93*0.57         1*141.90203
1*0.57              30*0.57          93*0.57             1*417.784455    93*0.57         1*171.978343
1*0.57              93*0.57          93*0.57             1*430.806528    93*0.57         1*205.880608
1*0.57              93*0.57          93*0.57             1*442.194532    93*0.57         1*239.667274
1*0.57              93*0.57          93*0.57             1*452.068349    93*0.57         1*276.684582
1*0.57              93*0.57          93*0.57             1*460.399317    93*0.57         1*303.794306
1*0.57              93*0.57          93*0.57             1*468.965817    93*0.57         1*323.858723
1*0.57              93*0.57          93*0.57             1*478.044668    30*0.57         1*341.907633
1*0.57              93*0.57          93*0.57             1*486.212985    1*345.829695    1*363.791224
1*0.57              93*0.57          93*0.57             1*494.605977    1*358.708718    1*386.532674
1*0.57              93*0.57          30*0.57             1*502.34791     1*377.51783     1*1000000
1*0.57              93*0.57          1*364.001797        1*509.253577    1*391.927965    1*386.532674
1*0.57              --3              1*378.310423        1*515.858164    1*403.26558     1*363.791224
1*0.57              93*0.57          1*400.830788        1*521.068074    1*412.079428    1*341.907633
30*0.57             93*0.57          1*418.207771        1*1000000       1*420.296837    1*323.858723
93*0.57             93*0.57          1*431.279099        1*521.068074    1*427.121896    1*303.794306
93*0.57             93*0.57          1*442.720907        1*515.858164    1*433.538345    1*276.684582
93*0.57             93*0.57          1*452.693206        1*509.253577    1*440.564205    1*239.667274
93*0.57             93*0.57          1*461.936063        1*502.34791     1*447.680753    1*205.880608
93*0.57             93*0.57          1*471.042647        1*494.605977    1*454.6881      1*171.978343
93*0.57             93*0.57          1*480.501201        1*486.212985    1*461.365401    1*141.90203
93*0.57             93*0.57          1*490.695342        1*478.044668    1*468.147658    1*119.937604
93*0.57             93*0.57          1*500.027323        1*468.965817    1*474.93525     1*106.33594
93*0.57             30*0.57          1*508.345134        1*460.399317    1*480.631473    1*100.288517
93*0.57             1*349.633584     1*515.591508        1*452.068349    1*1000000       1*100.030006
93*0.57             1*362.15341      1*522.376395        1*442.194532    1*480.631473    1*103.985618
                                                         1*430.806528    1*474.93525     1*113.560104
```

Figure B.3: Permeability distribution in the reservoir, including conductivity distribution for the fracture face.